GROWTH OF GLIOBLASTOMA XENOGRAFTS IN THE BRAINS OF NOD/SCID MICE FOLLOWING ADMINISTRATION OF A DEMYELINATING AGENT

by

Mireille Kayitesi Johannessen

Master Thesis in pharmacy

Department of Biomedicine/Centre for Pharmacy
University of Bergen
June 2011

ACKNOWLEDGEMENT

This thesis is part of my studies for the Master degree in pharmacy at the Centre for Pharmacy, University of Bergen. The practical work was carried out at the Department of Biomedicine, University of Bergen, in the period from August 2010 to June 2011

I would like to express my gratitude to my supervisor Per Øyvind Enger (Institute for Biomedicine) for his guidance and support throughout the year. I am also grateful for having been introduced to his group which has been an inspiring and motivating multidisciplinary team. Many thanks go to all members of this group, especially Ercan Mutlu for his support in this thesis.

I would like also to thank Linda Sleire and Per Øystein Sakariassen for reading and commenting the manuscript, Cecilie Brekke Rygh and Tina Pavlin for teaching me how to use MRI scanner. Many thanks also to Øyvind Torkildsen, Stig Wergeland, Bø Lars for all cooperation in this thesis, all workers in the animal facility at Vivarium Center (University of Bergen), for their help and support throughout my time here.

I am thankful to my family for their love and encouragement. To my Mum, Dad, sisters and brothers for their cheering phone calls and good advice.
Last but not least, my gratitude goes to my husband Steinar Johannessen for his care and unconditional love, my beautiful daughters Alexandra U. Johannessen and Sophie T. Johannessen, for their understanding and patience during my study. I will be forever indebted.

Mireille Kayitesi Johannessen, Bergen 2011

ABBREVIATIONS

ABC: Avidin-Biotin-Complex
APL: Acute promyelotic leukaemia
BBB: Blood-brain barrier
CSF: Cerebral spinal fluid
DAB: 3, 3-diaminobenzidine
dH_2O: Distilled water
DMED: Dulbecco's modified eagles' medium
DNA: Deoxyribo nucleic acid
EAE: Experimental autoimmune encephalomyelitis
EDTA: Ethylenediamine tetra acetic acid
EGFR: Epidermal growth factor receptor
FELASA: Federation of European laboratory animal science associations.
FBS: Fetal bovine serum
FLAIR: Fluid attenuated inversion recovery
FOV: Field of view
GBM: Glioblastoma multiforme
i.c: Intra-cranial
IDH1: Isocitrate dehydrogenase 1
IHC: Immunohistochemistry
MIC: Molecular imaging centre
MRI: Magnetic resonance imaging
$N0_2$: Nitrogen dioxide
MS: Multiple sclerosis
NEAA: Non essential amino acids
IVC: Independent ventilated cages
HIF: Hypoxia-inducible-factor
LM: Light microscopy
MAG: Myelin associated glycoprotein
NOD/SCID: Non-obese diabetic severe combined immunodeficient
NK cell: Natural killer cell
OPC: Oligodendrocyte progenitor cell
PBS: Phosphate buffer saline
PPMS: Primary progressive multiple sclerosis
PRMS: Progressive/relapsing multiple sclerosis
RARE: Rapid acquisition with relation enhancement
RRMS: Relapsing-remitting multiple sclerosis
SPMS: Secondary progressive multiple sclerosis
TBS Tween: Tri-buffered saline Tween
TCGA: Cancer genome atlas
TE: Time echo
TMEV: Theiler's murine encephalomyelitis virus
TR: Repetition time
UV: Ultra violet
VEGF: Vascular endothelial growth factor
WHO: World Health Organisation

ABSTRACT

Background: Glioblastoma multiforme (GBM) is an incurable and fatal brain cancer with short median survival. Due to the infiltrative growth into the surrounding brain parenchyma, radical surgery is not possible and their infiltrative growth patterns provide one of the biggest challenges to effective treatment. However, quite few experimental therapies targeting tumor invasion have been performed and none have prolonged survival in patients. An important mechanism underlying infiltrative growth involves the migration of tumor cells along myelinated nerve fibres (white matter tracts). Cuprizone is a neurotoxic demyelinating agent which is used to study autoimmune diseases of CNS in immunocompetent mice. Since myelinated nerve fibres provide a substrate for glioblastoma cell migration, we hypothesized that cuprizone could inhibit the infiltrative growth of glioblastoma xenografts. Since highly infiltrative brain tumor models are based on xenografting human GBM biopsies, this requires an immunodeficient host such as nude rats or SCID mice. However, whether the cuprizone model for demyelination can be established in immunodeficient strains is not known. Thus the work presented in this thesis describes the establishment of cuprizone model for demyelination in NOD/SCID mice. Subsequently, we used the model to investigate the effect of cuprizone on the growth of GBM xenografts.

Method: Four NOD/SCID mice above 18 kg of weight, 4-8 weeks of age, both male and female were fed cuprizone to analyse if it caused demyelination. All mice were offered a daily portion (5 g per mice) of standard mice diet mixed with 0, 2 % cuprizone and were provided with water ad libitum. MRI was taken two, four, six and eight weeks after adding cuprizone to the diet. One brain was harvested at each time points for MRI scanning and fixed in formalin for histopathological analysis and immunohistochemistry. This analysis confirmed progressive demyelination during the diet, indicating that the cuprizone model could also be established in NOD/SCID mice. We then administered cuprizone to five more NOD/SCID mice that had been xenografted with GBM spheroids one week prior to starting the diet. These mice were compared to mice harboring GBM xenografts that received a regular diet. We then performed a second experiment where five additional mice were put on a Cuprizone diet two weeks prior to implanting them with GBM spheroids. Again these were compared with control mice that were also implanted with GBM spheroids but received a normal diet without Cuprizone. Weight and survival data were collected and the brains were harvested and fixed for the histopathological analysis and immunohistochemistry (IHC).

Results: Our results demonstrate that NOD/SCID mice exhibit cuprizone-induced demyelination of the corpus callosum, progressive hydrocephalus and depletion of oligodendrocyte precursor cells. Mice that were xenografted with GBM spheroids one week prior to staring the cuprizone diet did not show prolonged survival compared to the control group. However, mice that received cuprizone before GBM implantation had a significantly longer survival than the control mice. Moreover, immunohistochemistry showed less infiltration of proliferating tumor cells in the tumor periphery, as well as recruitment of microglia to both the tumor centre and periphery.

Conclusion: The present study has proved that cuprizone-induced demyelination in NOD/ SCID mice provides an adequate animal model to investigate how demyelination impacts on the growth of GBM xenografts. Moreover, IHC against tumor proliferating cells after inducing demyelination show that the myelin sheaths are important substrates for glioma cell migration. Prolonged survival in the cuprizone group also suggests that interactions between glioma cells and the myelin sheaths are targets for anti-invasive glioma therapy. However, the therapeutic potential of cuprizone is highly questionable, due to its toxic effects. In contrast, novel compounds that block the attachment of glioma cells to the myelin sheath without causing structural damage, may have a big potential as anti-invasive compounds for gliomas.

Table of contents

1. INTRODUCTION

1.1 General aspects of cancer

Cancer is a disease in which cells with genetic aberrations exhibit uncontrolled growth. Although the cell of origin is not known, it is known that cancers develop clonally. They arise from one cell which passes its mutations on to the daughter cells *(2)*. Full malignant transformation requires several genetic changes which are often acquired step-wise over several years (3-5). The affected cells can be classified into oncogenes and tumor-suppressor genes (6). Oncogenes are mutations in genes that normally promote cell growth (proto-oncogenes). Thus oncogenes are gain-of-function mutations where increased amounts of proteins or altered activity contribute to tumor progression. Oncogenes are dominant as mutation in one allele is sufficient to promote tumor growth. On the other hand, tumor-suppressor genes suppress cell growth and induce apoptosis. In cancers, tumor-suppressor genes are often inactivated leading to increased cell proliferation and disruption of apoptotic pathways. Thus, these genetic changes are referred to as loss-of-function mutations. Tumor-suppressor genes are recessive since mutations in both alleles are required.

Most cancer types share some common defining traits. These traits are indentified as phenotypic hallmarks of cancers (7-9) :

- **Growth signal autonomy:**

  Cancer cells do not rely on external growth factors but are self-sustained with growth-promoting signals

- **Avoidance of growth inhibitory signals:**

  Cancer cells exhibit resistance to growth inhibitory signals

- **Evasion of apoptosis:**

  Cancer cells evade apoptotic signals

- **Unlimited replicative potential:**

  Cancer cells exhibit the ability for indefinite growth and cell division

- **Sustained angiogenesis:**

  Cancer cells induce growth of new blood vessels to secure a sufficient supply of oxygen and nutrients

- **Invasion and metastasis:** Cancer cells have the ability to invade surrounding tissue and spread to distant body parts.

Over the past decade, the perception of tumor biology has evolved revealing the necessity for establishing further cancer hallmarks which allow the cancer cells to grow and invade healthy tissue. The cancer cell's capabilities to manipulate their stroma to create a favourable microenvironment are additional changes needed for mutated cells to grow and spread. The cancerous cells may need to reprogram the cellular energy metabolism, or to actively dodge from the attack and the eradication by immune cells in order to sustain survival and growth. Cancer cells also exhibit genomic instability and obtain increasingly more genetic aberrations during the disease course (8). This new biological perception of cancer indicates that cancer should not be viewed as a cancer cell–isolated pathogenesis, but rather as a disease involving a complex interaction with other cells in the microenvironment. Furthermore, this up-to-dated understanding of tumor biology indicates the need for a modern therapeutic approach in order to control the disease.

In recent years, the cancer stem cell hypothesis has been postulated. According to this concept, tumors contain small subpopulations of cells that have the ability to self-renew as well as to differentiate into other tumor cell types with a more limited replicative potential. Thus the cancer stem cells drive tumor progression and create the cellular heterogeneity seen in many tumor types. Reportedly, cancer stem cells have been indentified in several tumor types, such as leukemias (10-12) and brain tumors (13-18). However conflicting data have been published by several groups (19-21) and this concept is a controversial issue.

1.2 Glioblastoma multiforme (GBM)

Glioblastoma multiforme represent the biggest group of primary bran tumors. They are classified by their similarity to the glial cell types, and graded by their degree of malignancy. Glioblastoma multiforme is the most common and aggressive malignant primary brain tumor. They can not be radically removed due to their infiltrative growth and radio- and chemotherapy prolong survival only modestly. Thus, GBMs have a dismal prognosis with almost 100% mortality rates and a short median survival in the range of ca 14 months (22). The incidence of GBM is about 2-3/100 000/year, and they are slightly more common amongst men. The only established risk factor is ionising radiation. Histopathologically, they are characterised by mitotic figures, cellular atypia, necrosis, and microvascular proliferation (angiogenesis).

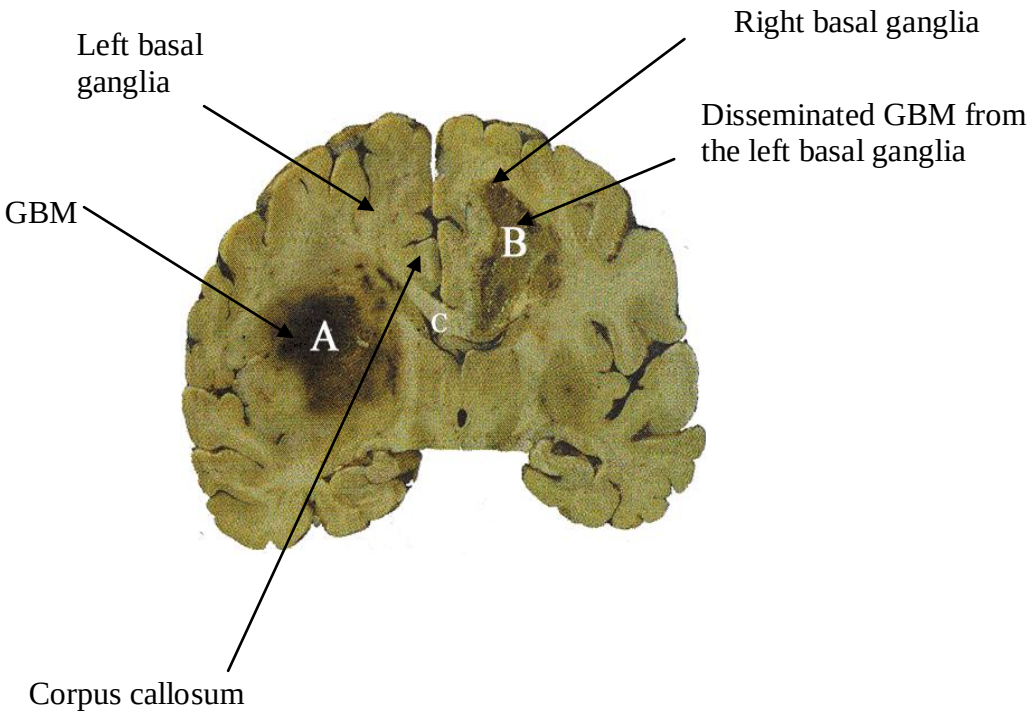

Fig: 1.2: A coronal section of a GBM. The figure shows a primary lesion in on the left basal ganglia followed by a secondary lesion in the right hemisphere due to the migration of cancer cells across the corpus callosum. The figure is adapted from P. Kleihues (23)

Moreover, glioblastoma can develop in patients not previously diagnosed with a brain tumor (GBM) or from a more low-grade glioma (secondary GBM).

1.2.1 Primary and secondary glioblastoma multiforme

GBMs are genotypically heterogeneous and there is no single mutation that is common to all GBMs. However, many mutations are seen in varying proportions of GBMs. It has also been proved that primary (low grade) and secondary (high grade) GBMs develop through different genetic pathways. They have different rates of anaplastic progression and are observed in patients of different ages (24) .

Secondary GBM harbour TP53 mutations and usually affect younger patients. The progression from low-grade glioma through an anaplastic astrocytoma and finally a GBM may take 10-15 years. In contrast, primary GBMs develop in older patients and typically involve loss of heterozigozity of 10q (70% of cases), EGFR amplification (36%), p16(INK4a) deletion (31%), and PTEN mutations (25%) (25). The high grade GBMs are more common than secondary GBMS (> 90 %) (25, 26).

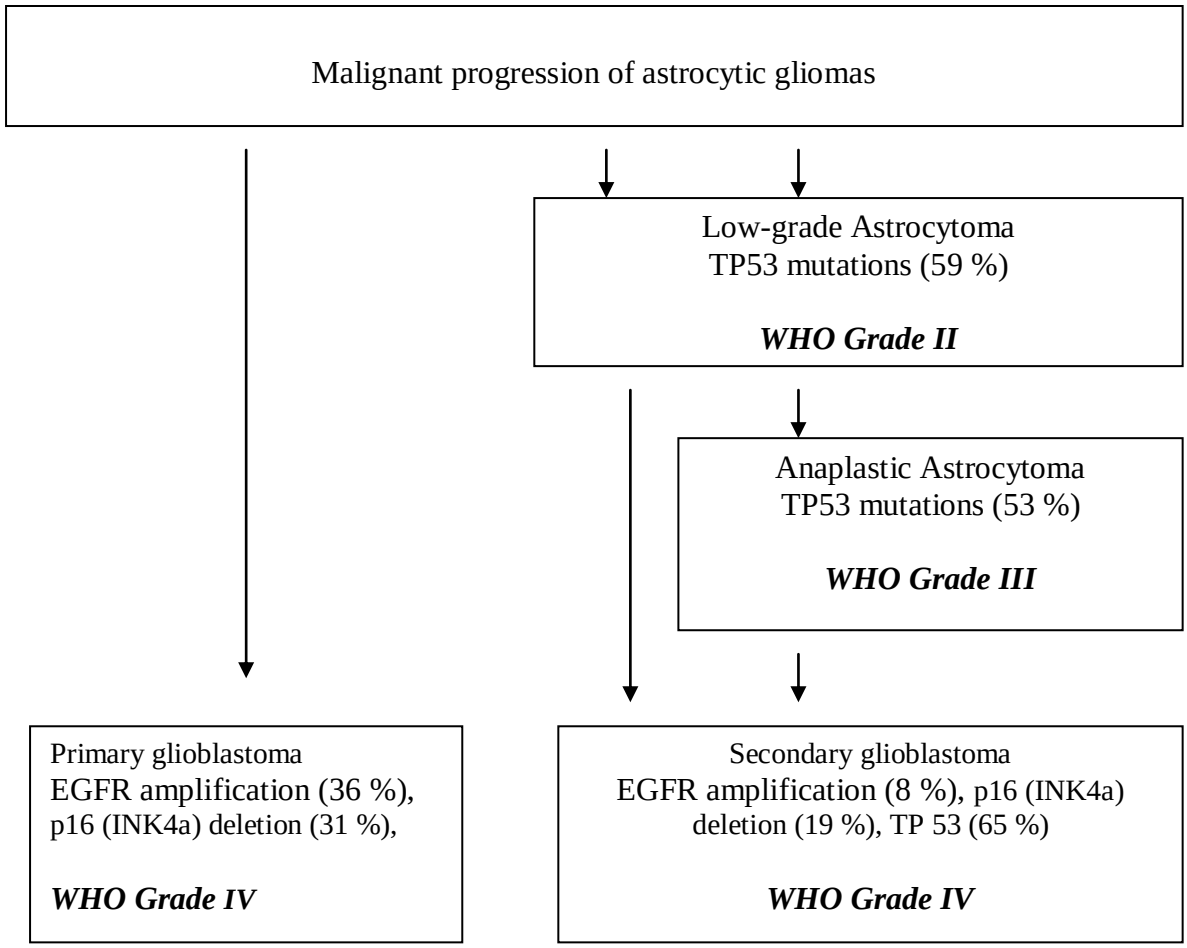

Figure1. 1: A sketch showing genetic alterations associated with the development of GBMs. The WHO grading system is added. The World Health Organization (WHO) classifies the primary brain tumors into four grades, based on various histological features, and to their resemblance of cells of origin within the CNS (27, 28). WHO Grade I, II astrocytomas (respectively Pilocytic and diffuse acystroma) are characterised by a very low level of proliferation, while grade III (anaplastic astrocytoma) exhibits diffuse anaplasia, a relatively high degree of mitotic activity and proliferation as compared to grade I and II. Grade IV (glioblastoma multiform) exhibits a high diffuse infiltration and necrotic areas in the centre of the tumor masse. The frequencies of the genetic alterations are shown as percentages. Figure modified from Ohgaki and Kleihues (25).

During the past decades, the grading of gliomas has relied on the WHO classification system, based on various histological features and the resemblance of tumor cells with the main CNS types. However, DNA sequencing and gene expression profiling have identified GBM subgroups that correlate with different survival outcome. The Cancer Genome Atlas (TCGA) data has been used to identity subgroups in human gliomas (29). In addition, results from the recent cohort study using the genomic sequential method in gliomas (29, 30), grouped GBMs into proneural, classical and mesenchymal probable GBM subtypes. Mutations within these groups are currently used as markers for prognosis. For example mutated IDH1 and mutated TP53 have been observed to be associated with improved survival in subgroups of young patients (30). However, gene expression is also influenced by epigenetic alterations such as

metylations which are not detected by sequencing (31). Thus, methylation and gene expression analysis can provide additional information about the biology of gliomas.

1.2.2 Glioma cell invasion and biological mechanisms

The GBM is the fastest growing type of astrocytoma and quickly spreads and invades nearby normal brain tissue. They rarely spread to other parts of the body (2, 32), but invade locally by realising factors that modulate the CNS microenvironment which, in return, accommodates their motility (33-35). The GBM invasion employs interactions between malignant cells, glial cells, neural cells and endothelial cells involving proteolytic enzymes, cell adhesion molecules and specific cell surface receptors (36). Notably, the tumor-stroma interplay mediates the spread of the glioblastoma cells into other regions of normal brain parenchyma (37) by migrating along the white matter fiber tracts such as the corpus callosum (38, 39). In addition, tumor cells may be passively distributed with the cerebrospinal fluid to distant sites within the CNS such as the spinal medulla.

1.2.3 Glioblastoma multiforme (GBM) therapy

As previously mentioned, GBMs are incurable due to their infiltrative growth. The existing treatments can prolong survival by months and decrease the symptoms (brain oedema, headaches, seizures, different types of neurological deficits, etc.). Several centres advocate a standard treatments of GBMs that include maximal resection of > 95% of the tumour, followed by adjuvant concurrent chemotherapy and radiotherapy, and maintenance therapy with temozolomide depending on predictive and prognostic factors (22, 40, 41). This approach is still under survey, and it is suggested that the results might improve the median and 5-year survival with 3-5 % for the patients. Several novel molecular target therapies for GBMs are also under investigation, including HER1/EGFR tyrosine kinase inhibitors (Gefitinib, Erlotinib), angiogenesis inhibitors (Bevacizumab), mTOR inhibitors (Everolimus Rapamycin, Deforolimus and Temsirolimus), and farnesyl transferase inhibitors (42). However, none of these have yet prolonged survival for patients in randomised clinical trials.

1.3 Multiple sclerosis

Multiple sclerosis (MS) is a chronic inflammatory neurodegenerative disease affecting the oligodendrocytes with their myelin sheaths around the axons of neurons in the central nervous system (CNS) (43). The myelin sheath plays an important physiological roll, serving as insulation around the nerve fibres in the human central nervous system, and is necessary to increase the transmission speed of the electrical signals. Thus, demyelination inhibits propagation of action potentials along the axons, disrupting the communication between neurons in the CNS.

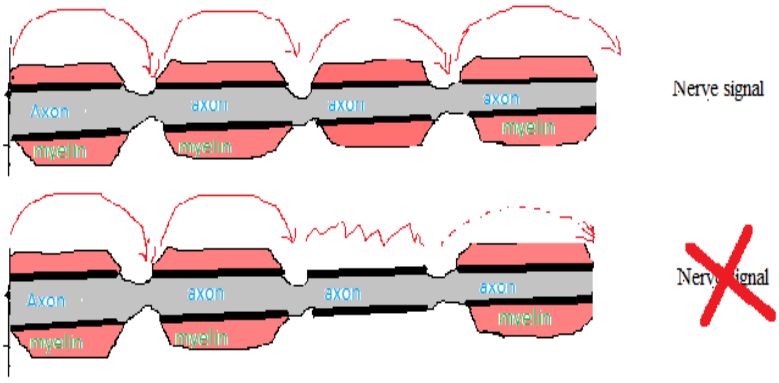

Figure 1.3: The pathogenesis of multiple sclerosis: demyelinated neuronal axon leading to interruption in nerve impulse.

The abnormal communication between the brain and the rest of the body leads to different neurological symptoms of multiple sclerosis (44). Thus, multiple sclerosis is characterised by plaques in affected regions, inflammation, axonal injury and progressive physiological disability. It mostly develops in people between 20-40 years and it is 2-3 times more common in women than in men (45). In Norway there are about 5000 to 8000 who are affected by the disease (46). The aetiology of the disease in human is not known, but potential causes includes genetic, infections, physical and emotional stress, climate and diet (47).

1.3.1 The pathology and the pathological subgroups of human multiple sclerosis

The immunological processes causing multiple sclerosis is not fully understood (48), but they target the oligodendrocytes and the myelin (49). In the early stage, the inflammatory process involves microglia, macrophages , B-cells, their antibody products and T-cells in the central nervous system (50). It is often followed by disruption of the blood-brain barrier (BBB) (48, 51), allowing proliferating T- and B-cells to migrate across the BBB into the CNS. These attacks lead to thinning or complete loss of myelin (52). The restoration of the myelin (remyelination) can occur during the early progression of the disease (acute inflammatory

lesions), followed by a functional recovery and clinical remittance. However, the oligodendrocytes can not completely rebuild the myelin sheet, thus repeated attacks ultimately leaves a scar and axonal injury/loss (53). The progression of multiple sclerosis disease differs from person to person. Based on the clinical course, MS is classified into three main clinical groups (46, 54-56):

- Relapsing-remitting MS (RRMS); representing the initial course of the disease and characterized by discrete attacks evolving over days to weeks (rarely over hours). The symptoms appear in episodes of exacerbations (relapses) and it may take months or years between relapses.
- The secondary progressive MS (SPMS) is the course after RRMS; the presenting symptoms increase gradually to become chronic.
- The third course refers to primary progressive MS (PPMS) where patients have gradually increasing symptoms from the onset without remissions. The disease is characterized by steady deterioration leading to continuous increase in neurological deficits without clear relapses or periods of remission.
- The progressive/relapsing MS (PRMS) overlaps PPMS and SPMS.

1.3.2 Toxic demyelination models allowing to study MS pathology in animal experiments

The neurodegenerative demyelination in MS disease have been mimicked in the animal model producing similar histopathology changes (57). Three models for demyelinating diseases are widely used, namely EAE (58), Theiler's virus induced encephalitis, and toxic demyelinating model (48, 59). In EAE, immunization with myelin antigens induces inflammatory demyelination in the CNS. In Theiler's virus induced encephalitis, the mice are infected with the neurotropic picornavirus, leading to the demyelinating disease. In the toxic demyelinating model, chemical agents such as lysolecithin, ethidium bromide, or cuprizone are used to induce demyelination. The cuprizone is a commonly used model to study corpus callosum demyelination (60).

Table1.1: Description of four different pathological patterns in early MS-lesion. Pathological features of early lesions in different animal models used for investigating MS in humans (61-63)

Patterns	Pathological characteristics	Mediating factors in human MS	Experimental animal model allowing to study MS pathology
I	Demyelinated plaque, T-lymphocyte and macrophage dominated inflammation with relative preservation of oligodendrocytes	Macrophage or/and their toxic products	Autoimmune encephalomyelitis (AEA)
II	The patterns resembles pattern I, and has additionally Ig reactivity	Specific demyelinating antibodies and compliments	Autoimmune encephalomyelitis (AEA)
III	Active demyelination, complement activation , preferential loss of myelin associated glycoprotein (MAG), lesions are infiltrated with T-lymphocytes, macrophages and activated microglia	Degenerative changes in oligondrocytes followed by apoptosis (myelin sheath are not targeted)	Therapeutic model using toxin – induced demyelination
IV	Roughly demarcated plaques of demyelination, olygodendrocytes death exposed by DNA fragmentation.	Primary degeneration of oligodendrocytes followed by myelin destruction (myelin sheath are not targeted)	Therapeutic model using toxin – induced demyelination

1.3.2.1 Cuprizone, a copper chelator agent

In mice, cuprizone can be used as a model for toxic demyelination (64). The demyelinating effect of cuprizone is mediated by its copper chelating chemical reaction targeting directly oligodendrocytes, leading to progressive loss of oligodendrocytes (65). However, the underlying mechanisms of cuprizone-induced toxic effects on oligodendrocytes in CNS are not fully understood. It has been suggested that the cuprizone binds copper in the oligodendrocyte cellular membrane and that subsequent depletion of cupper ions which are vital for enzymatic activity in the mitochondria leads to myelin damage.

It has been shown that the cuprizone neurotoxic effect is strain dependent (66), and the C57BL/6 mice is now frequently used for demyelination/remyelination studies as it

recapitulates the neuro-pathological patterns similar to those observed in the human multiple sclerosis disease (48, 57, 62, 63, 66-77). They appear in form of focal lesions in the corpus callosum region, followed by recruitment of microglia. The myelin loss occurs as a consequence of primary loss of oligodendrocytes, and remyelination, mediated by oligodendrocyte progenitor cells (OPCs) can occur upon withdrawal of cuprizone treatment (78). However, the lack of myelination and chronic persistent MS lesions following depletion of oligodendrocyte progenitor cells can also be studied with prolonged cuprizone treatment more than 8 weeks. The toxic effect of cuprizone also cause radiological and structural changes in the CNS of C57BL/6 mice, such as dilated ventricles (hydrocephalus) in the brain parenchyma (65).

1.3.3 Multiple sclerosis therapy

Multiple sclerosis disease is an incurable disease. However, a number of treatments for acute attacks, or for reduction of the biological activity (disease-modifying agents) are obtainable. The drugs like corticosteroids can be used in acute exacerbation of the disease to improve symptoms and shorten time of disability and the immunomodulatory treatment using interferon for example, can be used to slow the destruction of myelin. In addition, different symptomatic treatments can improve symptoms such as cognitive loss, depression, paranoid, visual disturbances, etc (symptomatic treatments). The medical treatments for MS which are available do not cure or prevent the disease, but they rather reduce the disease activity, limit disability and delay disease progression (79). Findings suggest that an individual therapeutic approach is efficient, reducing the clinical relapses and associated inflammation in the CNS, and delaying the disease deterioration and subsequent disabilities (79). Thus the current therapies, combined with high standards of care, may offer the patients a normal life span.

1.4 NOD/SCID mice models

The animal models for cancer research are generally based on any of three approaches: chemical induction, transgenic animal models or xeno-transplantation models (80), the latter often involving immunodeficient mice to study tumor (81). Moreover, the xeno-transplantation model have been used in clinical research, testing potential pharmaceutical agent and the success has rendered this technique an important tool in pharmaceutical commerce (82). Severe combined immunodeficiency (SCID) mice carry a homozygous mutation causing a lack of functional B-and T-cells. In addition, the mutation in these mice is transferred onto non-obese

diabetic (NOD) background to avoid the development of partial immunity (leakiness). Due this deficiency, the mice allow for engraftment of human tissue (80), such as cancer cell lines or tumor biopsies (83). Previously, experimental representative brain tumor models derived from human GBM biopsies have been established in NOD/SCID mice. However, NOD/SCID mice have not to our knowledge been validated as a host model to study demyelination.

2. AIM OF THE STUDY

Glioblastoma multiforme is an incurable disease due to its infiltrative growth. The myelin sheath around the nerve fibers provides a substrate for migration of glioma cells. Multiple sclerosis is a demyelinating disease affecting the oligodendrocytes and their sheaths. Relatively few reports of MS patients diagnosed with GBM have been reported. Thus we wanted to investigate whether demyelination could inhibit tumor growth and invasion.

The aim of the work was:

1- To establish an animal model for demyelination in NOD/SCID mice using cuprizone.

2- Administer cuprizone to NOD/SCID mice grafted with GBM biopsy spheroids to investigate how the demyelination impacts on tumor growth.

3. MATERIAL

3.1 Mice

Table 3.1: Description of the mice used in this experimental study

SPECIES	Mus musculus, inbreeding laboratory mice
STRAIN *(international nomenclature):*	NOD/SCID
SOURCE	Local breeding at the Vivarium
GENETIC STATUS *(if not obvious from stock/strain designation)*	Homozygous for *Prkdc*^{scid} genotype and the dsred reporter transgene
AGE and/or WEIGHT *at start of experiment*:	3-8 weeks; 15-35 g
SEX	Male and female
MICROBIOLOGICAL STATUS	The mice are tested in accordance with the FELASA requirements(84). Every 3 months 10 animals from the sentinel animal population should be subjected to a full microbiological and pathological examination.
QUARANTINE or ACCLIMATIZATION Since this is local breeding, the mice are in the same facility throughout their life span. They are transferred to the cages used for the experiments 1 week prior to the start of the experiments.	
HEALTH MANAGEMENT OF ANIMALS UNDER ***Measures to protect microbiological status*** Closed system IVC cages ***Housing equipment (types, material, dimensions, possibly cage type)*** IVC cages (73 X 65 X 13) cm ***Number of animals per cage or housing unit:*** 4-6 mice ***Bedding***: The bedding is delivered from Scanbur BK and is routinely tested to ensure that its content does not affect the experiments. In addition the environment is enriched with different other materials including paper and plastic elements. ***Environment temperature (0c -+ range), relative humidity***: Temperatures is maintained in the range 18-22 ℃. ***Lightning:*** 12 light/12 dark cycles is used. Entrance to the mouse room and lightning during the dark cycle is avoided. ***Air changes per hour:*** 18 ***Feeding***: The food pellets, called "RM1" rodent maintenance diet containing wheat, barley, de-hulled extracted toasted soya, soya protein concentrate, macro minerals, soya oil, whey powder, amino acids, vitamins and micro minerals. ***Water:*** Tap water ad libitum.	

3.2 In vivo experiments

Table 3.2.1 Chemicals

Chemicals	*Catalogue number*	*supplier*
Isofluran	J109020	Schering Plough Animal Health, Ballerup, Denmark
Marcain 2.5 mg/ml	-	AstraZeneca, Södertälje, Sweden
Cuprizone	C9012-25G	Sigma-Aldrich, co, Austria
Omniscan 0,5 mmol/ml	107789930	GE Healthcare, Nycomed Amersham, Oslo, Norway

Table 3.2.2 Equipment

Equipment	*Supplier*
Stereotactic frame	David Kopf Instruments, Tujunga, CA, USA
Temperature controller	World Precision Instrument (WPI), Inc.
Germinator 500	Cell point scientific, Gaithersburg, MD, USA
Sutures	Ethicon, Norderstedt, Germany
Surgical sponges	Neurotechnics limited, Oxfordshire, UK
7T MR scanner	Bruker Biospin MRI GmbH, Ettlingen, Germany

Table 3.2.3 Cell biopsy

Spheroids	Cell type	Supplier
P3	Human Glioblastoma	Haukeland University Hospital, Bergen, Norway

3.3 Cell culture

Table 3.3.1 Chemicals

Chemicals	*Catalogue number*	*Supplier*
Dulbecco's modified eagle's medium (DMEM)	D5671	Sigma-Aldrich Inc, St. Louis USA
Dulbecco's phosphate buffered saline 10X (PBS)	BE17515F	Sigma-Aldrich Inc, St. Louis USA
L_Glutamine (Gln)	BE17605E	Cambrex, New Jersey, USA
Non-essential amino acids (NEAA)	BE13114E	Cambrex, New Jersey, USA
Penicillin/Streptomycin (PenStrep)	DE17603E	Bio Whittaker Inc, Walkersville, USA
Plasmocin	ant-mpt	InvivoGen, Calfornia, USA
Trypsin	17161	Lonza Walkersville Inc, Walkersville, USA

3.4 Apparatus and software

Equipment	*Supplier*
Lamin Airflow cabinet	Het-Holten A/S, Denmark Medionor ASA
Light-microscope Olympus IX2-SLP	Olympus, Tokyo, Japan
Light-microscope Nikon Eclipse E600	Nikon, Tokyo, Japan
MRI scanner	Siemens Magneton vision, Erlangen, Germany

3.5 Immunohistochemistry

Table 3.5.1: chemicals

Chemicals	*Catalogue number*	*Supplier*
Citrate buffer	W302600	Sigma –Aldrich, Belgium
TBS Tween buffer (TBST) 10X	S3306	DakoCytomation, Glostrup, Denmark
Peroxidase block buffer	547500	DakoCytomation, Glostrup, Denmark
DAKO protein block	S3022	DakoCytomation, Glostrup, Denmark
DAB chromogen and DAB solution/buffer	Acu-250	DakoCytomation, Glostrup, Denmark
Ethanol	600068	Arcus Kjemi, Vestby, Norway
Harri Hematoxylin solution	RBA-4213-00A	Kjemi-Teknikk as, Norway
Heating bath	HBR4	IKA Werke, GmbH & Co, Staufen, Germany
Xylene	33817	Sigma-Aldrich Inc, St. Louis, USA
EDTA	ED2SS	Sigma-Aldrich, Inc, St. Louis, USA
ABC-complex	PK - 7100	Vector Laboratories, Burlingame
Entellan Neu	1079610100	Merck KGaA, Darmstadt, Germany
Luxol fast blue	MBSN-1328-51-4	ChemExper Inc., Belgium.

Table 3.5.2: Antibodies

Antibodies	*Dilution*	*Catalogue number*	*Supplier*
Primary antibodies			
Ki-67 mouse-monoclonal	1:100	M7240 00045312	DAKO Cytomation, Glostrup, Denmark
NG2 rabbit-polyclonal	1:100	AB81104	ABCAM, Cambridge, UK
CD68 mouse-monoclonal	1:100	M081401	DAKO Cytomation Glostrup, Denmark
Secondary antibodies			
Goat anti-mouse	1:100	1070-11L	Southern Biotech, Birmingham, Alabama, USA
Goat anti-rabbit	1:100	BA_1000	Vector Laboratories, Burlingame

4. METHODS

4.1 Mice strain

NOD/SCID mice, male and female, with a minimum of weight of 18 g were used. All laboratory procedures involving mice were in accordance both with the guidelines implemented by the Ethical committee / National Animal Research Authority (NARA). The animals were sacrificed by gas stunning (asphyxiation by CO_2), followed by cervical dislocation.

4.2 Study design and cuprizone treatment

4.2.1 Cuprizone test in SCID mice

Four NOD/SCID mice, 4-8 weeks of age, both male and female were fed 0, 2% cuprizone to analyse if cuprizone induces demyelination in central nervous system, a similar pathological pattern observed in established animal models for human multiple sclerosis. MRI was taken on the second, forth, sixth and eighth week after cuprizone administration and the brain from one mouse was harvested and fixed in formalin at each scanning and was cryosectioned for immunstaining and histopathological analysis. All mice were offered a daily portion (5 g per mice) of standard mice diet mixed with 0, 2 % cuprizone and were provided water ad libitum.

4.2.2 Experimental therapy targeting invasion of GBM

19 mice, 4-8 weeks of age, both male and females were grouped randomly into 2 groups: one intervention group (n=10) and one control group (n=9). These groups were further divided into 2 experiments, in which cuprizone treatment was started at different time points (see below):

Experiment I		Experiment II	
Intervention approach mimicking the therapy after diagnose, where cuprizone was administered one week after gliomas implantation		Intervention approach where the therapy is targeting gliomas invasion, and cuprizone was administered 3 weeks before glioma implantation	
Cuprizone groupe	***Control group***	***Cuprizone groupe***	***Control group***
5 mice	4 mice	5 mice	5 mice
9 mice		10 mice	

All untreated groups in each category were fed normal diet and provided water ad libitum while the treated groups were offered a daily portion (5 g per mice) of normal diet mixed with 0, 2 % cuprizone. The MRI for all mice in each experimental group was taken on six and eight weeks after cuprizone administration. Apart from the diet, the same protocols for implantation, pre- and post-operative procedures were applied in all animals.

4.3 Biopsy tissue collection

The GBM biopsy was harvested with the informed consent of patient at the operation theatre at the Department of Neurosurgery, Haukeland University Hospital. The use of human biopsies in cancer research is approved by the Regional Ethical Committee. The specimen was collected using a standard procedure (85) as follows: the biopsy was taken from tumor areas appearing macroscopically viable, corresponding to regions with contrast enhancement on preoperative magnetic resonance imaging (MRI) scans and immediately transferred under aseptically conditions to test tubes containing a complete growth medium, which consisted of DMEM, supplemented with 10% fetal bovine serum (FBS), 2% L-glutamine, and 4× the prescribed concentration of nonessential amino acids, penicillin, and streptomycin.

4.4 Tissue culture and spheroid cells preparation

From the GBM biopsy material, tumor spheroids were prepared as previously described (85). In short, samples were minced into 0.5-mm fragments, placed into 80-cm^2 tissue culture flasks (Nunc, Roskilde, Denmark), and base coated with 10 mL of 0.75% agar (Difco, Detroit, MI) in culture medium (DMEM). The spheroids were maintained in a standard tissue culture

incubator with 5% CO_2 in air and 100% relative humidity at 37°C and the medium was changed once weekly. After 1 to 2 weeks in culture, spheroids with diameters between 300 and 400 µm were selected for i.c. implantation. The spheroids used in this experiment were established from GBM xenografts using the same procedure as described above for making GBM spheroids.

4.5 Anesthesia

Inhalation of Isofluran 5% (Schering Plough Animal Health, Ballerup, Denmark) combined with N_2O was used as general anesthesia, and 0, 2 ml 0.1 % marcain was injected subcutaneously in the scalp as a local anesthesia about halfway between the ears. Before implantation, the mice were anesthetized in an induction chamber supplied with 5 % isofluran. The isofluran dosage was adjusted to 2-3 % during surgery. The respiration and the body temperature of animal under anesthesia were monitored and regulated using a temperature controller with a heating plate and a rectal probe, keeping the rectal body temperature of the mouse at approximately 37 ^{0}C.

4.6 Injection of glioma spheroids

Five tumor spheroids (300-400 micrometer in diameter) were selected under light microscope (Nikon, Tokyo, Japan) using a 50 µl syringe. The spheroids used in the last experiment were somewhat bigger than the spheroids in the first experiment, due to limited availability. When the animal was unconscious it was immobilized in a stereotactic

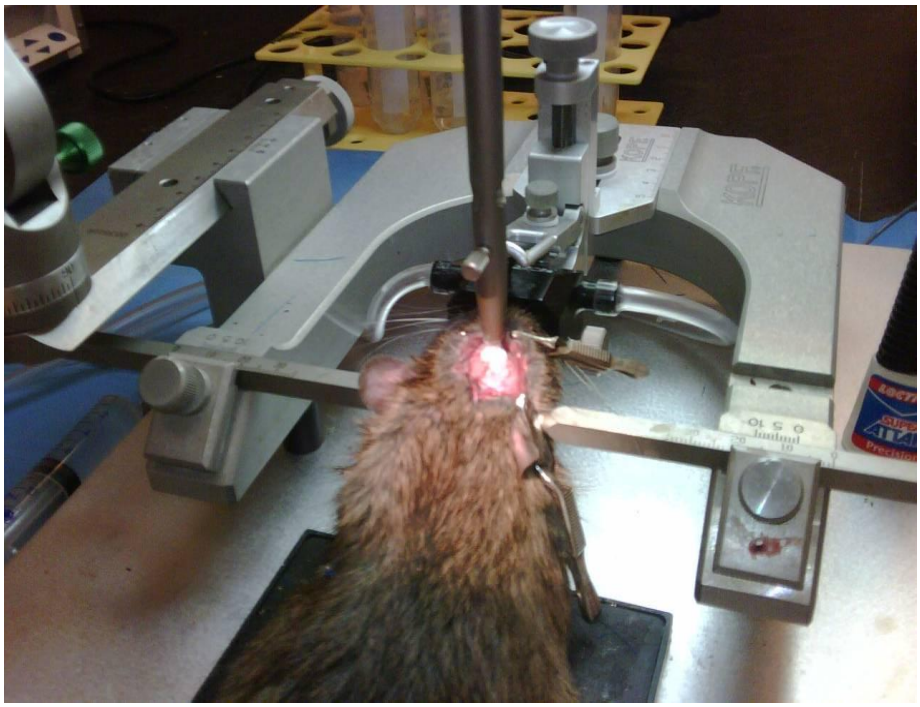

Figure 4.1: Animal immobilized in a stereotactic frame during surgery.

frame and the head locked in position with ear and nose bars as shown in figure 4.1.

During the course of spheroids injection, the mice lied on a heating pad which was connected to a thermometer that was put into the mice' s rectum, and we made sure that the mice had a constant body temperature of 37 degrees Celsius. An incision was made in the skin to access the skull, starting behind the eye going caudally 2 cm. The skin was held away from the exposed skull with one bulldog clip on each side of the incision. The point where bragma and sutura sagittalis meet was then located (figure 4.2). A whole in the bone was drilled at the coordinates: x= 1.5 mm right of the sagittal suture (midline), y= 0.5 mm behind the bragma suture. A cell suspension was injected over 1-2 minutes with a mikroliter syringe z= 1.5 mm under the cortical surface. The skin was carefully closed with three sutures. The mice was then released from the nose and ear bars and moved to an infant incubator where it was kept until to wake up.

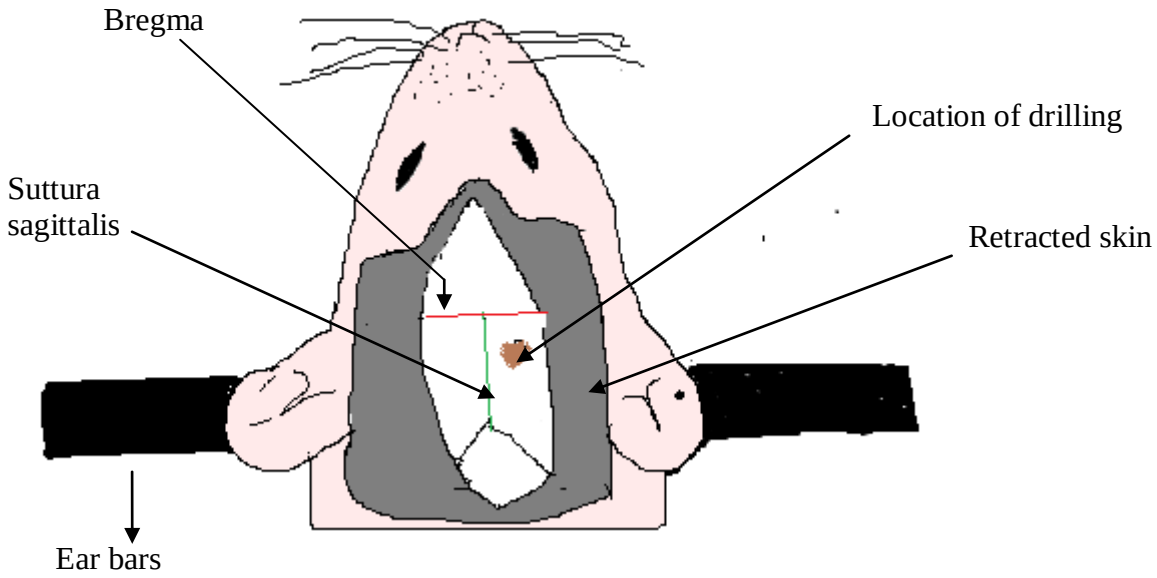

Figure 4.2 –The point of drilling through which injection of tumor cells was done is marked with a brown dot. Adapted from Reference (1).

4.7 In-house small animal MRI scanner

The magnetic resonance imaging (MRI) was used to visualize the brain tumor and to study the structural changes in the mice brains. MR images were acquired using a 7T horizontal bore small-animal MR scanner (Pharmascan, Bruker Biospin) with a linear transmitter/receiver mouse-head volume coil. Animal were anesthetized using 1-2 % isofluran mixed with equal parts N2 and O_2 (50/50) supplied via a cone mask.

***Figure 4.3:** MRI scanner. The picture is used with permission from Molecular Imaging Center (MIC), University of Bergen*

All animals were placed in a prone position in the animal cradle containing a heating pad at 37 ^{0}C. Respiration was monitored throughout the experiment using dedicated animal monitoring equipment (SA Instruments).

The MRI protocols was as follows: MR sequences used include T2-weighted RARE sequence with TR/TE of 4200/35.2 ms, FLAIR sequence with TR/TE of 3200/9.2 ms and inversion time TI of 1500 ms, and T1-weighted RARE sequence before and after subcutaneous injection of contrast agent Gadodiamide (1.0 ml of 0.5 mmol/ml Omniscan mixed with NaCl (1:1); Nycomed Amersham, Oslo, Norway, Omniscan; GE Healthcare) with TR/TE 1000/9.0 ms. T1 and T2 weighted sequences had FOV of 2.0 x 2.0 cm and a matrix size of 256 x 256, while FLAIR had a FOV of 2.0 x 2.2 cm and a matrix of 256 x 256. 12 slices, each 1 mm thick were collected in all sequences. The combination of T1-, T2-weighted and FLAIR, sequences gave complementary information which allowed us to visualize the tumor structure and localize the tumor vicinity in the mouse brain.

4.8 Histological examination and immunohistochemistry (IHC)

In this study, we used luxol fast blue staining (LFB, ChemExper Inc., Belgium) to assess demyelination. Luxol blue stain was used to mark myelin fibers. Myelin fibers will appear blue following stain with LFB and can be observed under light microscope (57, 86).
Additionally, we performed immunohistochemistry (IHC). Different primary antibodies were used. Mouse monoclonal anti-Ki67 antibody (DAKO Cytomation, Glostrup Denmark) was used as cellular marker for human cell proliferation to determine the fraction of proliferating cells in the tumor bulk and to detect tumor cells. Rabbit polyclonal anti-NG2 antibody (ABCAM, Cambridge, UK) was used to identify oligodendrocyte precursor cells. Mouse monoclonal anti-CD68 antibody (DAKO Cytomation, Glostrup Denmark) was used to detect microglia and other macrophages.

4.8.1 Luxol fast blue (LFB) staining

The paraffin sections were deparaffinised by using toluol and hydrate to 95% ethyl alcohol and were then left in luxol fast blue solution in 56 ^{0}C ovens overnight. The slides were rinsed with 2-3 times in 95% ethyl alcohol. The sections were then rinsed in distilled water, before being dipped in 0, 5 % lithium carbonate for 15 – 30 seconds. Thereafter, the slides were rinsed in 2-3 times of 70 % alcohol. The rinsed slides were thereafter rinsed twice in distilled water. The sections were dipped four times in 70 % cresyl fiolet to stain the nuclei, followed by one dip in xylen 96 % (5sec), 1 dip in xylen 100 % (1 minute), and 1 dip 100 % (1 minute). Then the slides were mounted with xylene based mounting medium (Merck, Germany9 and were left to dry.

4.8.2. NG2; Ki-67; and CD68 staining

Paraffin sections of xenografted mice brain were stained using the manufacturer's protocol for immunostaining of paraffin sections Avidin-Biotin-Complex (ABC, Vector Laboratory, and Burlingame). Sections were deparaffinised by washing in xylol (2x5 minutes), 100 % ethanol (2x3 minutes), 96 % ethanol (2x3 minutes) and ddH_2O for 2 minutes. The sections were put in citrate buffer pH 6 and antigen retrieval was performed by heating at the boiling point for 20 minutes in a water bath. Sections were cooled down to room temperature under running tap water, dried, and washed with PBS-Tween (DAKO Cytomation, Glostrup Denmark). Peroxidase block buffer was applied for 5 minutes before sections were washed 3 times with PBS-Tween and incubated with protein block for 30 minutes. The protein block was

discarded and 50-100 µl primary antibody added (Ki-67 mouse monoclonal or NG2 rabbit polyclonal or CD68 anti-mouse) and incubated first for one hour at room temperature, and then 4^{o} C overnight in a humid chamber. All antibodies were diluted 1:100 in TBST/ 5% serum.

The sections were then washed three times in PBS-Tween. Goat anti-mouse antibody (Ki-67 and CD68) and Goat anti-rabbit secondary antibody (NG2) were added and sections were incubated at room temperature for ~45 minutes. Again, the sections were washed three times in PBS-Tween. Sections were then developed by adding 80 µl of DAB-solution (DAKO Cytomation, Glostrup Denmark) to each slide. The process was monitored under a light-microscope and stopped by adding dH_2O and washing with PBS-Tween when positive staining was visible, after approximately 3 minutes for NG2 and 45 seconds for Ki-67. The sections were placed in dH_2O until all the slides were developed. Counterstaining was performed by placing the slides in Hematoxylin for approximately 15 seconds, followed by rinsing under tap water. Finally, the sections were dehydrated trough 96 % ethanol (2x3 minutes), 100 % ethanol (2x3 minutes) and xylene (2x5 minutes) before they were mounted onto coverslides using xylene-based mounting medium. The slides were allowed to dry in a fume hood overnight.

4.9. Quantification of cells

Ki-67 index was determined by taking pictures of the tumor sections under a Nikon light microscope (Nikon, Tokyo, Japan) at x 40 magnification. A grid was applied over each picture using the Nikon software, with a grid size of 100 µm. All nuclei within 4 squares were marked and subsequently all Ki-67 positive nuclei were marked using a different colour. The fraction of all nuclei that was also Ki-67 positive was then calculated. Ki-67 index was calculated both in areas from the tumor bulk and in areas from the tumor periphery. Two tumors from controls and two tumors from Cuprizone treated mice were examined.

4.10 Statistics

Statistical analysis was performed using the GraphPad Prism 5 software. Weight curves were analysed during the repeated measures one-way Anova test. Survival analysis was conducted using the Log-rank test in two groups. A student t-test was used to test statistical differences between Ki-67 index for mice on standard diet vs. Cuprizone diet. Differences were accepted

as statistically significant at $p < 0.05$. Standard error of the mean are indicated in figures through the text.

5. RESULTS

5.1. Cuprizone effects in NOD/SCID mice

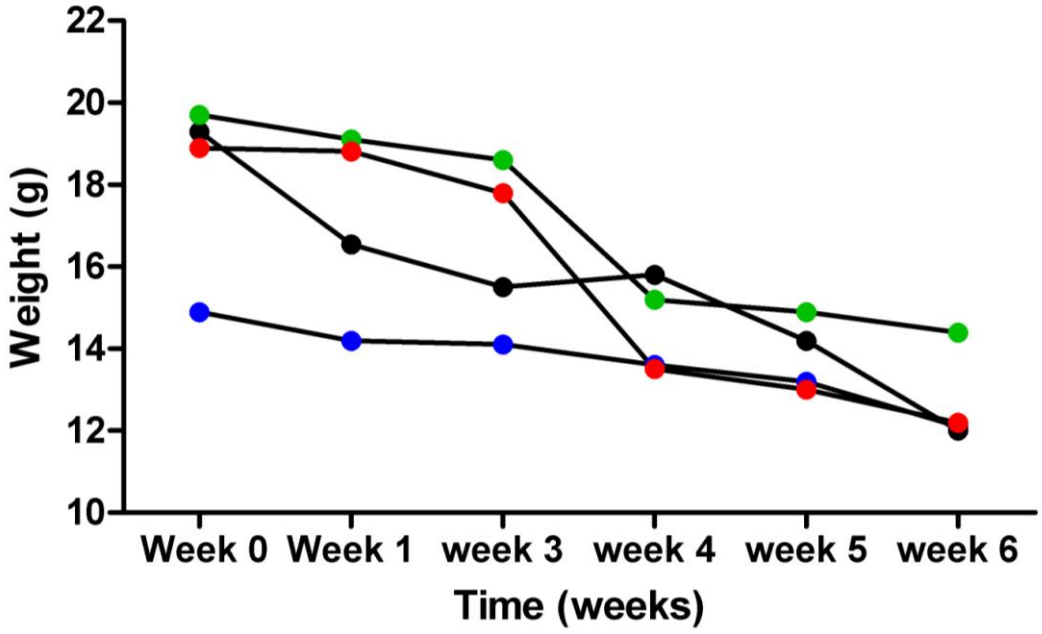

Figure 5.1.1: Weight loss during administration of 0.2 % cuprizone. 4 mice were given a daily diet of 5 g/mouse and their weights were recorded from start of the treatment (p = 0. 031)

In order to determine whether the cuprizone model for demyelination could be established in NOD/SCID mice, we first characterized the effects of cuprizone in NOD/SCID mice without tumors. As shown in figure 4.1, mice uniformly showed a significant weight loss. Although, the weight reduction varied within the group, there was a significant, approximately a 15 % average weight loss for the whole group (P = 0.031) following treatment with 0.2 % cuprizone

Moreover, we wanted to investigate if this mice strain exhibited the same radiological changes that were previously described in the C57BL/6 strain (48). Notably, NOD/SCID mice also showed increasing dilation of the ventricular system during the first 6 weeks (Fig. 5.1.2). However, the ventricular system was less dilated after 8 weeks. T1-weighted sequences after administering contrast agent did not show any contrast-enhancement (Data not shown).

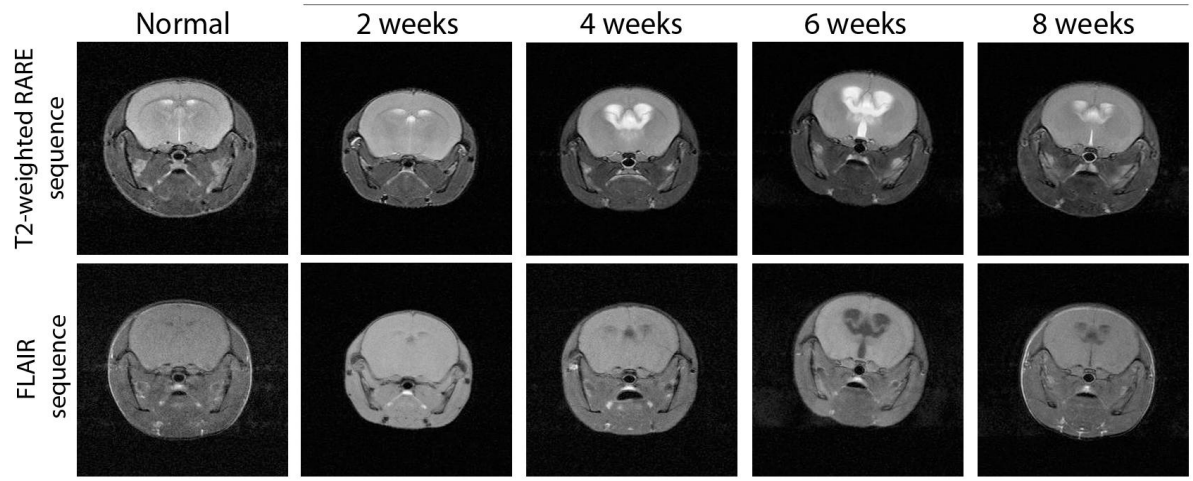

Figure 5.1.2: MRI coronary brain scans of NOD/SCID mice on normal diet and cuprizone diet at different time points. Upper panels: T2 weighted rare sequence, lower panels: FLAIR sequence. Both sequences demonstrate progressive dilation of the ventricular system (Hydrocephalus) up to 6 weeks (n=4).

In order to directly assess the effect of cuprizone on demyelination, we conducted luxol fast blue (LFB) staining of the mice brain sections and subsequently examined them under a light microscopy (Fig. 5.1.3). Luxol fast blue staining stains the intact myelin fibers in a strong blue colour.

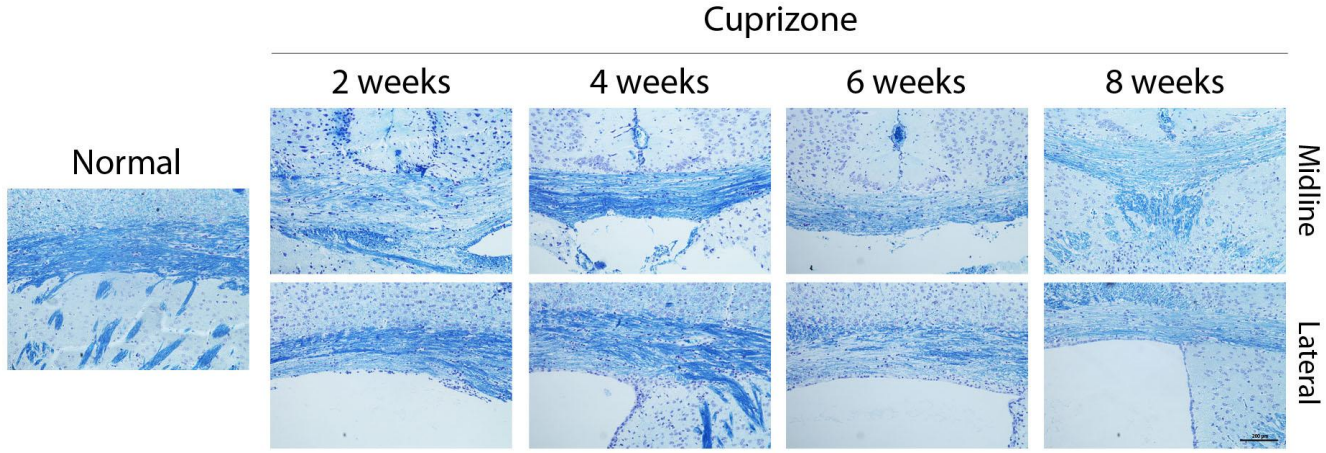

Figure 5.1.3: Luxol fast blue staining with (LFB) of NOD/SCID mice brains on normal diet and at different time points, as indicated, on cuprizone diet. Shown are coronary sections of Corpus Callosum in the midline (upper panels) and over the lateral ventricle which both exhibit progressive loss of myelin (n=2). Scale bar: 200 µm.

Although there were some variations, the overall pattern showed a progressive loss of myelin from 2 to 8 weeks. Thus, at the latest time point there was a striking thinning of the Corpus

Callosum compared to untreated control. This was apparent both in the thickest part in the midline as well as over the lateral ventricles.

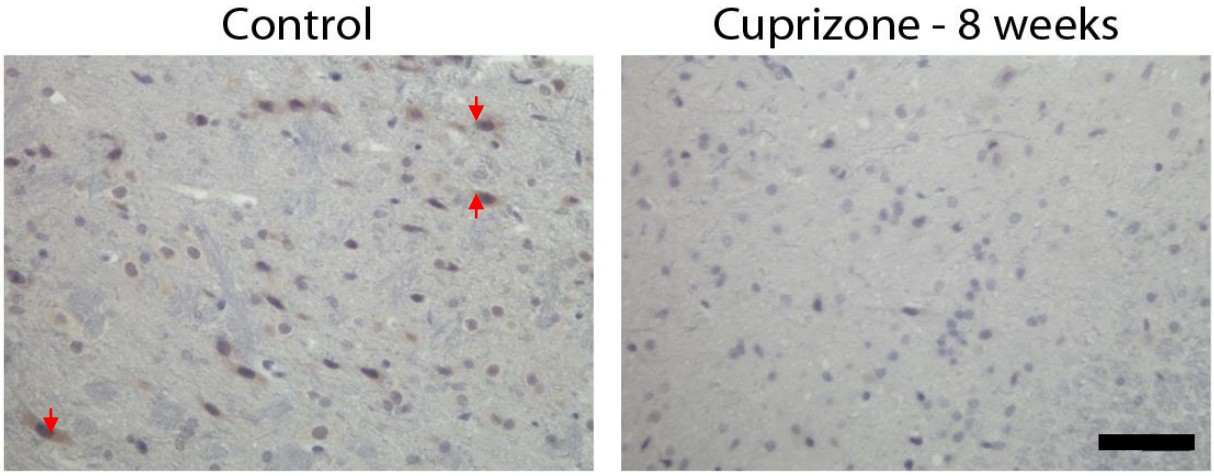

Figure 5.1.4: Immunohistochemistry (IHC) against NG2 (brown), a marker for oligodendrocyte precursors, nuclear counterstaining with Hematoxylin (blue). Whereas NG2-positive cells (arrowheads) are present in brains from untreated controls, mice brains are depleted of NG2-positive cells after 8 weeks of cuprizone treatment (n=3). Scale bar: 100 µm.

The potential for remyelination after cuprizone treatment relies on oligodendrocyte precursors reconstituting the pool of oligodendrocytes. Previously, Torkildsen *et al.* reported that oligodendrocyte precursors were depleted following 8 weeks of treatment with Cuprizone. Thus we performed IHC against NG2 of mice brains from animals treated with cuprizone for 8 weeks and untreated controls (figure 4.1.3). While numerous NG2-positive cells were present in normal brains, there was a striking almost complete loss of NG2-positive cells after 8 weeks treatment with cuprizone.

5.2. Cuprizone used as the therapeutic intervention in the glioma xenograft model

Since the myelin sheaths around nerve fibers provide an important substrate for glioma cell migration, we wanted to investigate whether cuprizone-demyelination impacted on the invasive growth of GBM xenografts and overall tumor progression.

5.2.1 On set of cuprizone treatment after implantation of GBM spheroids

In the first experiment, mice were first implanted with GBM spheroids and 0.2 % cuprizone was administered 2 weeks after implantation, whereas a control group were given the same diet without cuprizone. The mice were weighed once a week and revealed a significant weight loss in mice fed on cuprizone compared to control mice, starting from the 3rd week.

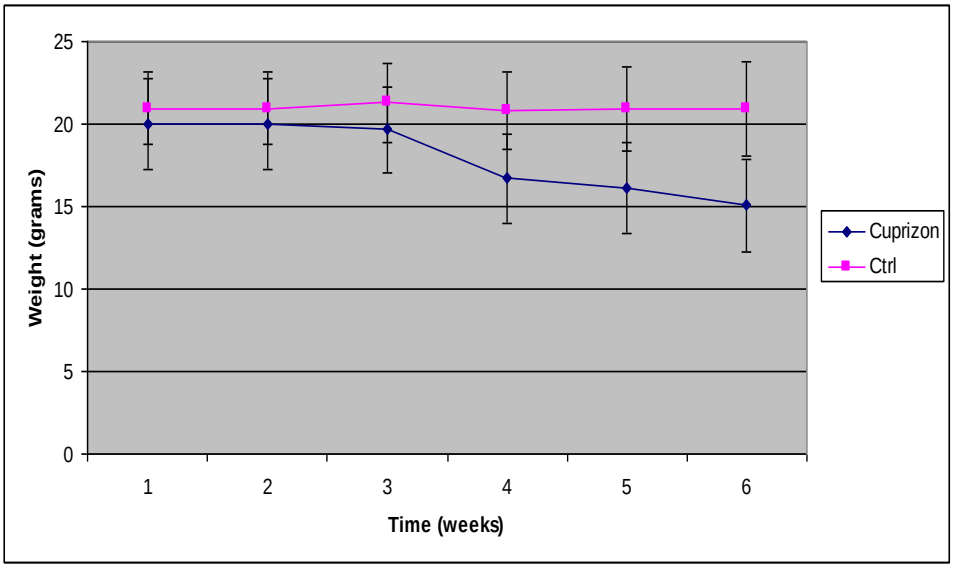

P = 0.19

Figure 5.2.1.1: Weight loss in tumor bearing mice fed on 0, 2 % cuprizone. (P=0.19, cuprizone diet: n=5, normal diet: n=4)

We monitored tumor growth in vivo using MRI, and confirmed tumor engraftment in both groups at 6 weeks. Like expected at 8 weeks, all tumors had clearly grown. Moreover, some control tumors had longer extensions on T1-sequences and more extensive oedema on T2-sequences. In contrast, some of the cuprizone treated tumors seemed more circumscribed.

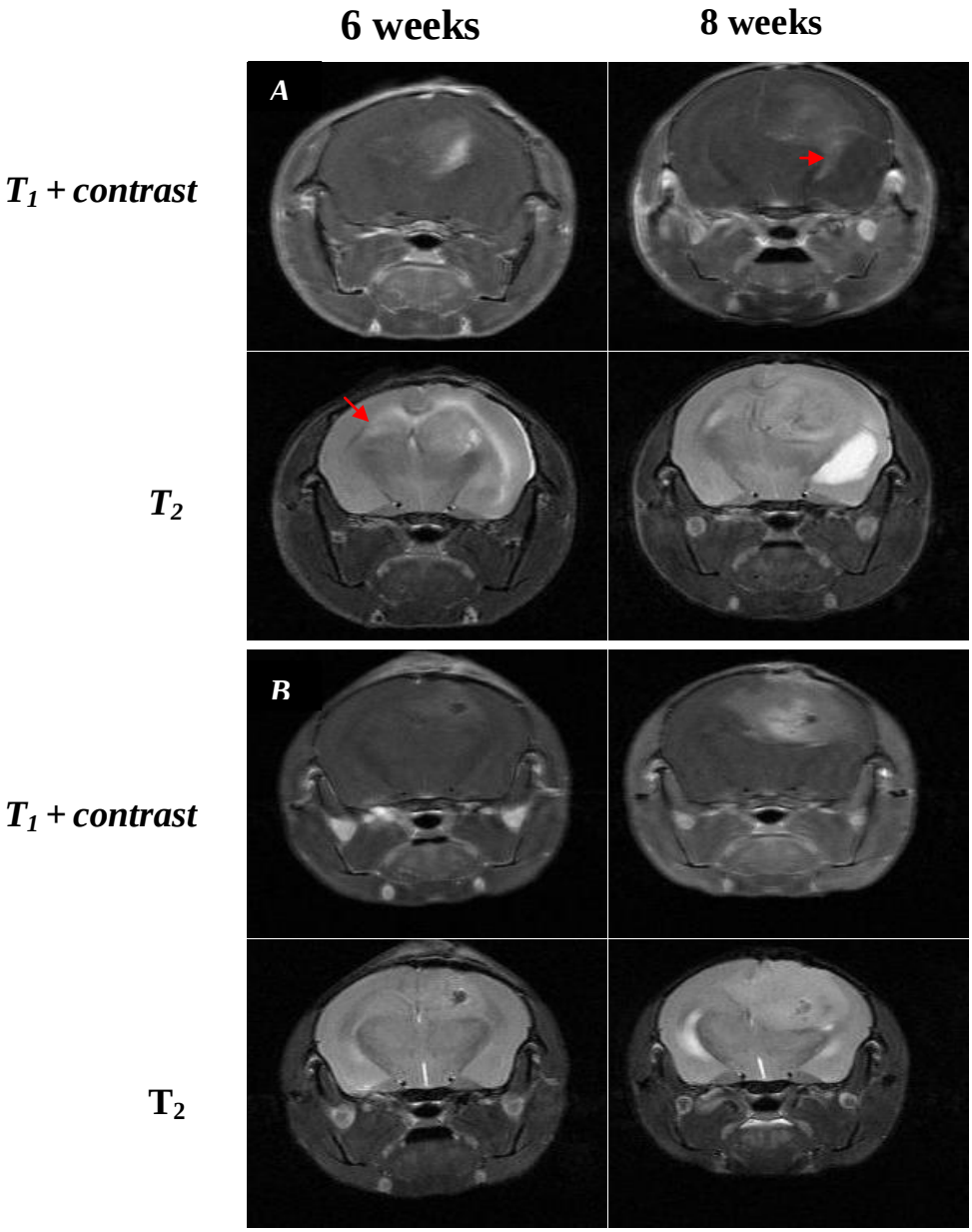

Figure 5.2.1.2: MRI brain scans of mice harbouring GBM xenografts on normal diet (A) vs. cuprizone diet (B), time points and imaging sequence as indicated. Tumor lesions are visible on T1-sequences as white/greyish lesions due to contrast enhancement. Note contrast-enhancing tumor extension (arrowhead) in control tumor A, upper right panel). Oedema is visualised on T2 sequences as high signal (lighter) areas. Tumor associated oedema (arrow) can be seen in control tumours into the contralateral hemisphere (A, lower left panel).

Also, we collected survival data for the animal which were sacrificed at the onset of symptoms. One animal in the treatment group died after 3 weeks before scanning, but did not show any tumor on histological examination. The two groups produced overlapping survival curves without significant differences ($p = 0.19$).

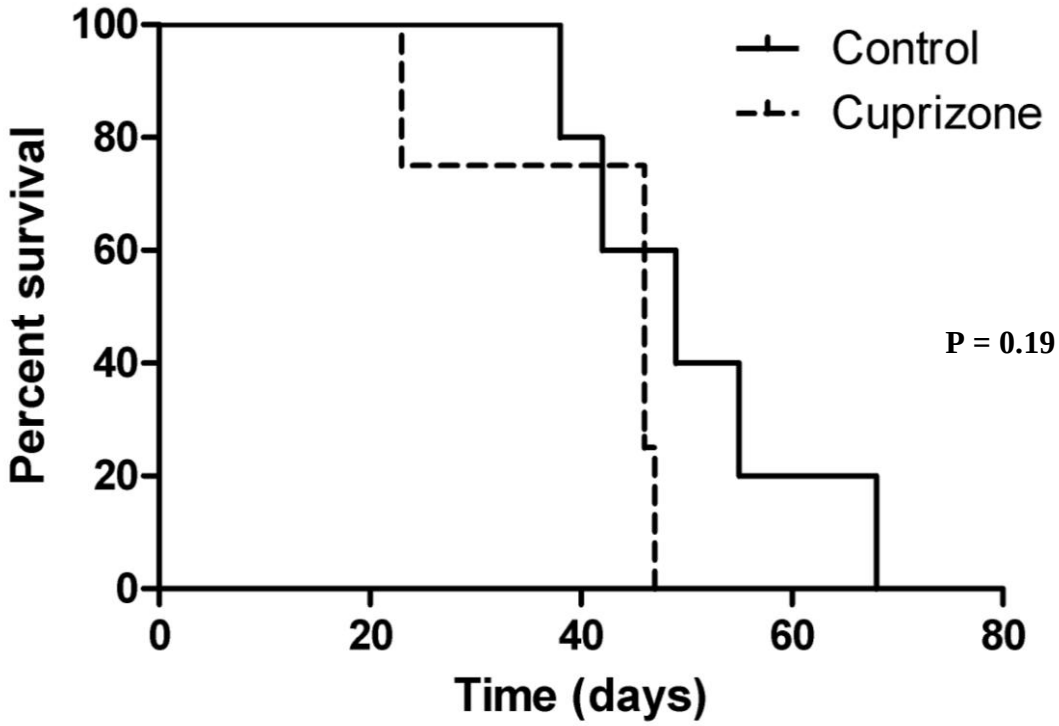

Figure 5.2.1.3: Survival from the time of implantation in mice harbouring GBM xenografts in NOD/SCID mice on normal or cuprizone diet (P=0.19)

5.2.2: Onset of cuprizone treatment prior to implantation of GBM xenografts

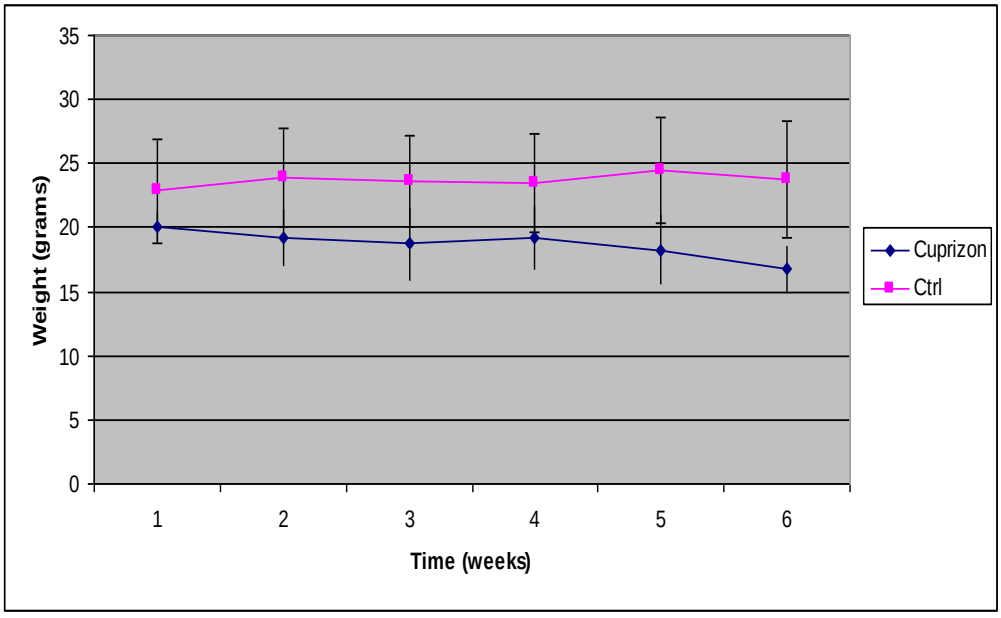

Figure: 5.2.2.1: Weight curves for mice on normal diet vs. 0.2 %cuprizone diet started 3 weeks before implantation of GBM spheroids. (P=0.045, cuprizone: n=5, controls: n=5)

In the next experiment, mice were fed 0.2 % cuprizone 3 weeks prior to implantation of GBM spheroids. The animals were weighed once a week and showed that cuprizone-treated mice experienced a significant weight loss compared to the control group after 6 weeks (p= 0.04).

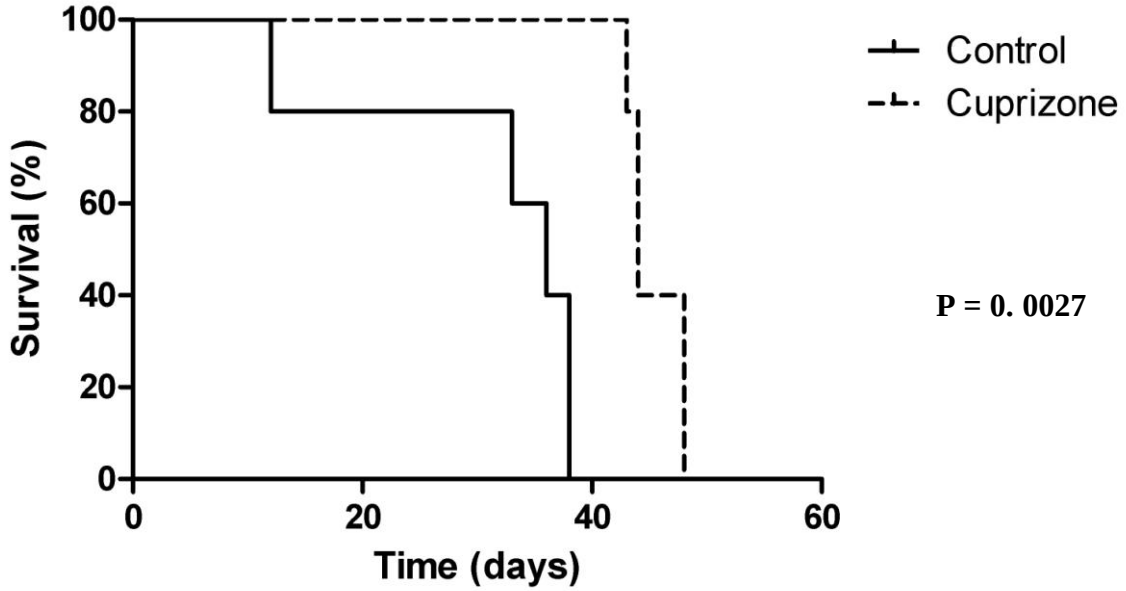

5.2.2.2: Survival from the time of implantation to the onset of symptoms in mice on cuprizone vs. standard diet (p= 0.0027)

Animals were sacrificed at the onset of symptoms, 12-48 days after treatment. Notably, all animals in the control group succumbed to their tumours 12-38 days after implantation of GBM spheroids. In contrast, animal on the cuprizone diet developed symptoms 43-48 days after implantation. Thus, animals on the cuprizone diet lived significantly longer than animals on a standard diet.

Since cuprizone treated animals lived longer, we performed IHC for the proliferation marker Ki-67 to investigate whether cuprizone inhibited glioma cell proliferation. For comparison, we assessed the fraction of Ki-67 positive cells in the tumor bulk from cuprizone treated tumors with controls. We found a relatively equal number of Ki-67 positive cells although there was slightly more Ki-67 positive cells in the cuprizone treated tumors, and the difference was not significant. Since the brain is largely a post-mitotic organ, we also used Ki-67 staining to identify proliferating tumor cells migrating along corpus callosum in the tumor periphery. Interestingly, this area showed a significantly higher infiltration of Ki-67 positive tumor cells in the control tumors compared to cuprizone treated tumors (p= 0.009)

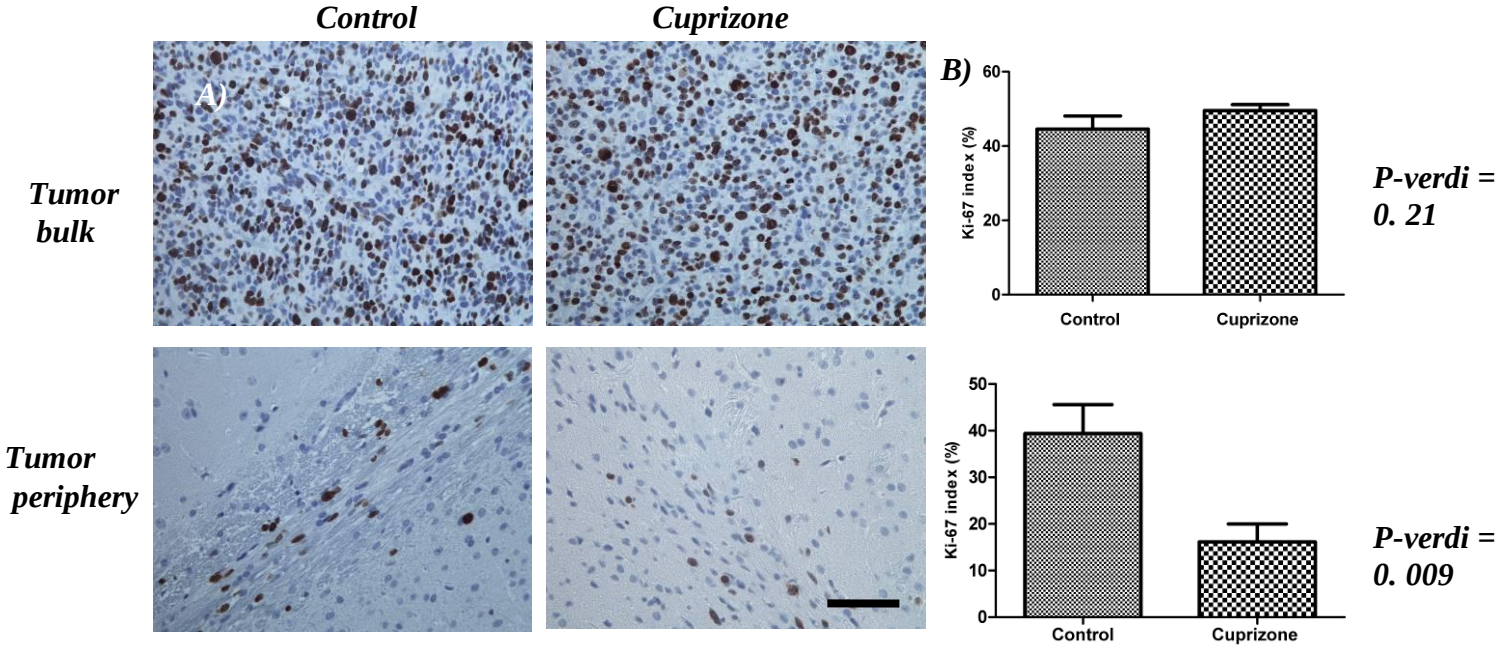

Figure 5.2.2.3: A) Immunostaining against Ki-67 (brown) in brain tumor sections from mice on standard vs. cuprizone diet. Nuclear counterstaining: Hematoxylin (Blue). Areas from the tumor bulk as well as the periphery were compared between mice on cuprizone vs. standard diet. Scale bar: 100 µm. B) Quantification of Ki-67 index between the two groups in areas from the tumor bulk (upper panel) and the periphery (lower panel). Scale bar: 100 µm

Since macrophages, including microglia are recruited both to tumors and areas of demyelination, we conducted immunostaining against the CD68-epitope, a marker for microglia and other macrophages (Fig. 5.2.2.4). In the tumor bulk (upper panels), there were numerous CD68-positive cells in both groups. However, there seemed to be more immunopositive cells in the bulk of cuprizone treated tumors (upper right panel). The invasion zone also contained CD68-positive cells, although these areas uniformly displayed a weaker staining (lower panels). Also in the tumor periphery, cuprizone-treated tumors seemed to contain more CD68-positive cells.

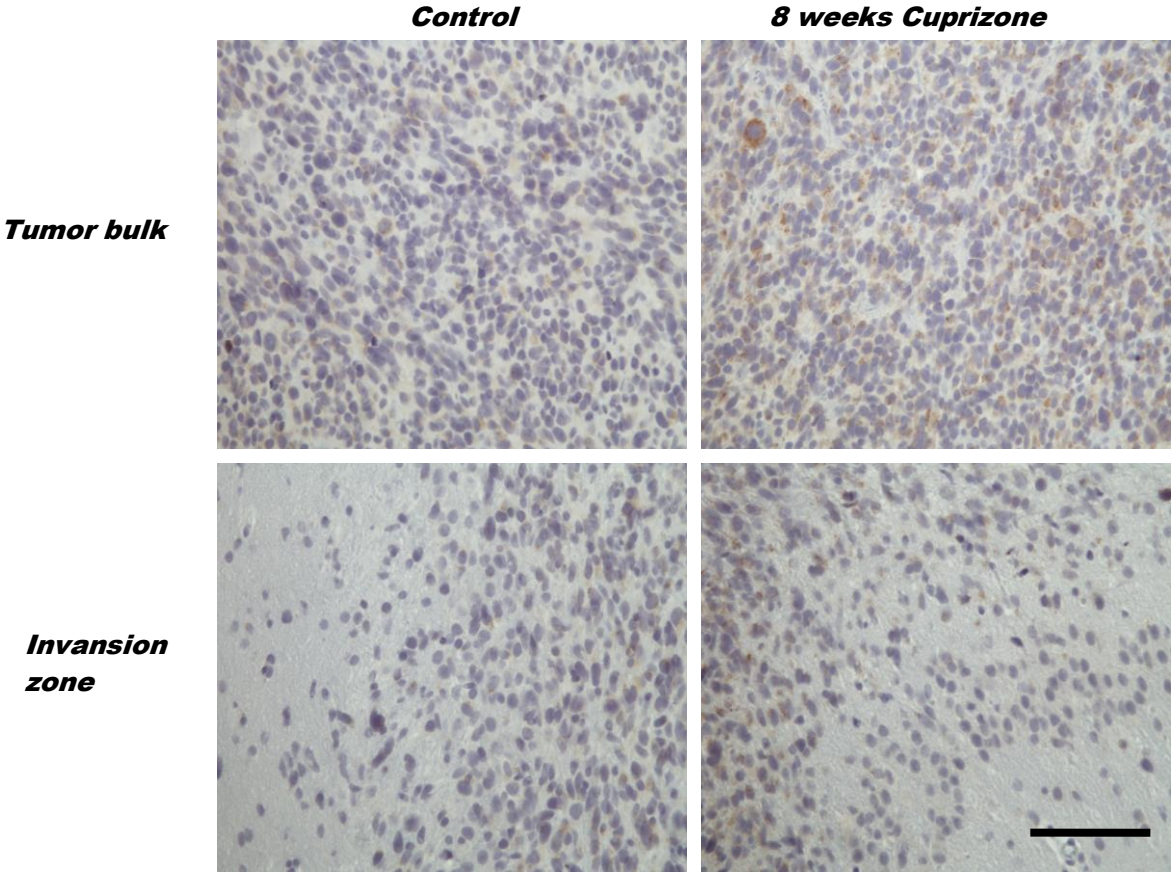

Figure 5.2.2.4: Immunostaining against CD68 (Brown) in areas from the tumor bulk (upper panels) and tumor periphery (lower panels) from cuprizone-treated tumors and control tumors. Nuclear counterstaining: Hematoxylin (Blue). Scale bar = 100 µm.

6. DISCUSSION

Cuprizone is a toxin which is used to induce demyelination in mice, thereby providing a model for multiple sclerosis. Its effect in rodent experiments is mediated through its copper chelating chemical reaction, targeting primarily the oligodendrocytes. Thus, the subsequent loss of myelin sheath is due to loss of oligodendrocytes (65) .The model is used to study autoimmune mechanisms underlying demyelination of the white matter tracts, and corpus callosum is the structure which is most investigated (60). In the present study, we wanted to investigate possible interactions between demyelination and invasion of human GBM xenografts. To allow engraftment of human biopsies we chose the immunodeficient NOD/SCID mice, which is not an established model for studying cuprizone-induced demyelination. Notably, NOD/SCID mice lack functional B- and T-cells whereas the cuprizone model involves autoimmune mechanisms. Thus, we first needed to assess whether this strain would exhibit demyelination in response to cuprizone treatment similarly to observations from the cuprizone model established in fully immunocompetent C57Bl/6 mice. If NOD/SCID mice showed the same response to cuprizone, we then wanted to study the biological role of myelin as a substrate for glioblastomas cell migration. From a clinical perspective, we also wanted to see if interactions between the tumor cells and the myelin sheet could be targeted therapeutically to inhibit glioma cell migration and prolong overall survival. The myelin sheaths are fundamental for proper functioning of the CNS, and a therapeutic benefit from demyelination therefore seems highly counter-intuitive. However, the history of medicine provides numerous examples of extremely potent toxins that have later been applied for medical purposes: The Botulinum toxin is now widely used for a variety of conditions, including corticollis (87, 88) as well as in cosmetics to improve wrinkles (Botox). Arsenic derivates have successfully prolonged survival in patients with acute promyelocytic leukaemia (APL) (89). Moreover, almost every drug is associated with some degree of toxicity, and especially cytotoxic agents used in cancer treatment are associated with potentially lethal side-effects.

6.1 The effect of Cuprizone in NOD/SCID mice

In the literature, demyelination in the corpus callosum of mice has been obtained following administration of 0. 2 % cuprizone (48, 62, 63, 66-74). The common hallmarks were shown in form of lesions in corpus callosum, axonal damage, hydrocephalus, myelin loss, depletion of oligodendrocyte progenitor cells (78), and recruitment of microglia into the affected areas (68,

76). Weight loss following cuprizone administration (74) has also been detected. In this work, we observed many of these traits, including weight loss, hydrocephalus on MRI, depletion of oligodendrocyte precursor cells (NG2) and recruitment of microglia (CD68).

The results from the weight records during administration of cuprizone (fig 5.1.1), showed that all mice uniformly lost weight, on average approximately 15 % of the weight at the beginning of the experiment. The weight loss was significant and in agreement with findings from previous studies (57, 74). However cuprizone mechanisms in association with weight loss are not known but findings suggest that (48), the weight loss following cuprizone treatment in SCID mice might be caused by cuprizone interference with the gastro-intestinal system of the mice.

The examination of the T2 weighted MRI 8 weeks after cuprizone administration (figure 5.1.2) revealed the presence of hydrocephalus and increasing dilation of the ventricular system. This is also in accordance with previous studies (48) and cuprizone may have contributed to weight loss and the fatigue symptoms observed in the mice. Although the cause of hydrocephalus is not fully known, it may be that inflammatory changes associated with demyelination compromise the re-absorption of cerebrospinal fluid.

The myelin loss was observed already from the second week of cuprizone treatment (fig 5.1.3), with almost complete demyelination towards 8^{th} week. However, we observed some variations as the brain harvested at 4 weeks stained stronger for myelin than the brain harvested 2 weeks after starting the cuprizone diet. This might reflect a partial remyelination as is seen in patients. In addition, earlier studies have demonstrated that partial remyelination of corpus callosum takes place at the second week after starting 0.3% cuprizone treatment (86), and 5,5 – 6 weeks after starting 0.2 % cuprizone treatment (78), while complete demyelination (apoptosis of regenerated cells) occurred from 4, 5 -5 weeks after 0.2 % cuprizone administration (78). Although our findings suggest that remyelination occurred earlier than what these studies reported, this difference may reflect differences between the model systems (NOD/SCID mice vs. C57Bl/6 mice). However, to fully characterise changes in the myelin sheath during treatment, this experiment will have to be expanded to include more animals at each time point. Due to the time constraints we were only able to do this experiment as a pilot. However, combined with the MRI findings and the IHC-results showing depletion of oligodendrocyte precursor cells we think this data collectively illustrate the effect of cuprizone clearly.

Along with myelin staining, we performed IHC against NG2, a marker for oligodendrocyte precursors, on brain tumor sections harvested 8 weeks after administering cuprizone. This showed almost a complete loss compared to brains harvested from control mice on normal diet. This suggests that the ability to reconstitute the pool of oligodendrocytes is lost after 8 weeks of treatment with cuprizone causing permanent demyelinated lesions (90). Although IHC can not be considered appropriate for quantifying subtle changes in expression levels, the difference between the brains from cuprizone treated mice vs. controls were striking. A more precise quantification of this difference can also be obtained with quantitative polymerase chain reaction (q-RT-PCR).

6.2. The effect of cuprizone on brain tumor progression

Cell migration along white matter tracts is an important biological mechanism underlying the infiltrative growth of gliomas and was already described in early neuropathological studies (91). Thus infiltrative growth and glioma cell migration along myelinated nerve fibres makes radical surgery impossible, and is the major cause of treatment failure. Whereas anti-angiogenic therapies have been validated in treating GBMs, specific anti-invasive drugs have yet not been designed. Having established that cuprizone induced demyelination in NOD/SCID mice we next wanted to investigate how demyelination impacted on glioma cell migration and overall growth. In our first experiment, mice were implanted with GBM spheroids and were fed cuprizone 1 week after implantation. This experimental design was chosen as it mimics the sequence of events in a clinical setting, in which patients are diagnosed with a tumor and then undergo therapy. In the second experiment mice received 0. 2% cuprizone 3 week prior implantation of GBM spheroids. Since demyelination was already present before the brains were implanted with tumor tissue, we decided this approach would optimal for investigating the role of myelinated fibres as in brain tumor invasion (38, 39).

In both experiments, the cuprizone fed mice lost weight compared to tumor bearing mice. One would think that the tumor bearing mice in control group might be affected due to their tumor burdon but this was not the case as these mice retained stable weights during the observation period. Mice that received cuprizone after the implantations had a slight shorter median survival (46 days) than control mice (49 days), but the difference was not significant (figure 5.2.1.3; $p = 0, 19$). Apart from the tumor burdon affecting both groups, it is possible that side

effects of cuprizone such as fatigue and hydrocephalus can have shortened the survival somewhat in the cuprizone group. In contrast, mice that received cuprizone prior to tumor implantation lived significantly longer than the control mice (figure 5.2.2.2; p = 0,002), and all control mice had been sacrificed before any mice in the cuprizone group developed symptoms. In studies such as these, the end point is estimated as the day the mice is dead or exhibit severe symptoms which lead to the sacrificing of the animal. The determination of end point is an ethical issue and differences between observers in interpreting the results may bias the results. In our experiment, it was mostly 2-3 individuals who inspected the animals daily. The person who inspected the animals daily belonged to the staff working at the animal facility and had not been involved in the experimental design. Thus, we believe the room for bias was limited

Although we used MRI to monitor tumor growth we were unable to measure tumor volumes since the contrast enhancement was often weak. Apart from that we didn't observe consistent differences between cuprizone treated and control tumors. However, some of the cuprizone treated tumors seemed more sharply circumscribed on contrast-enhanced T1 sequences and displayed less extensive tumor-associated oedema (figure 5.2.1.2). Thus the MRI findings suggested a less invasive growth in some of the cuprizone treated-tumors. In order to assess cell proliferation we performed IHC against the proliferation marker Ki-67 (figure 5.2.2.3) and found no significant differences in the tumor core between cuprizone treated and control tumors. Thus, the differences in survival could not be attributed to a cuprizone-mediated inhibition of tumor cell proliferation. In order to explore the possibility that cuprizone inhibited myelin-mediated tumor cell migration, we also examined the tumor peripheries. However, we had no pan-human specific antibody that reliably recognises all the human tumor cells established from this biopsy. Since the brain is largely a post-mitotic organ we also stained the tumor periphery for the Ki-67 epitope to detect proliferating tumor cells. Notably, cuprizone treated-tumors displayed a significantly less infiltration with proliferating tumor cells outside the tumor bulk (p-value = 0. 009). The limitation with using Ki-67 as a marker for tumor cells is due to its selectivity for actively cycling cells. Since only a fraction of the pool of tumor cells are actively proliferating, this method will not detect all tumor cells. However, the fact that the fraction of proliferating tumor cells in the centre of the tumors was similar in the two groups, it suggests that this limitation will affect both groups evenly. Thus, the immunostaining for Ki-67 suggests that the effect of cuprizone on overall tumor progression is mediated through its inhibitory effects on glioma cell migration.

Many studies have proved that there is a correlation between the elevated accumulation of macrophages (microglia) in cuprizone and CNS demyelination (48, 68, 86). Macrophages are present in cells of CNS during normal physiological condition but their amount can multiply when the brain get damaged (48, 57) following the cuprizone administration. Microglia cells have both neuroprotective, after acute neutoxicity (74) and neurodegenetive function during chronic toxic demyelination leading to axon damage (76). However, since demyelination is accompanied by inflammatory changes, it is also possible that this inflammatory environment have impacted on tumor cell invasion. Furthermore microglia are recruited both to neoplastic and inflammatory lesions in the CNS. We therefore performed immunostaining for the microglial marker CD68 on tumor sections from both groups, and examined both the tumor core and the tumor periphery (figure 5.2.2.4). Both control and cuprizone-treated tumors exhibited infiltration of CD68-positive cells, both in the centre and the periphery. Moreover, there seemed to be a stronger recruitment of these cells into the cuprizone treated tumors. This consistent with demyelination and inflammatory changes being important factors in attracting these cells. Again, IHC data are not suitable for investigating small differences in expression levels. Since, CD68-positive cells were also clearly present in control tumors this finding is uncertain and will ultimately need confirmation with more quantitative methods. One approach could be to dissociate the tumors into cell suspensions and quantitative the fraction of CD68-positive cells using flow-cytometry.

The findings in the present study indicate that the therapeutic method commencing cuprizone intervention 3 weeks before GBM implantation has a significant effect on gliomas invasion and that myelin play a role in facilitating GBM cell invasion. Like previously mentioned, this is in agreement with evidence from previous histopathological studies shoving that invasion of gliomas into other regions of the brain parenchyma follows the white matter fiber tracts of corpus callosum to the contra lateral hemisphere of the brain (38, 39). This again suggests that the myelin can be a target in glioma infiltrative invasion to the brain parenchyma.

6.3 Conclusion

- NOD/SCID mice exhibit demyelination in response to cuprizone and display weight loss, depletion of oligodendrocyte precursors and hydrocephalus similar to what has been reported for other mice strains. This provides a novel model to study how impacts on human glioma cell migration demyelination.
- Onset of cuprizone treatment one week after implanting glioma spheroids did not prolong survival in NOD/SCID mice.
- Cuprizone treatment started 3 weeks before implantation of glioma spheroids significantly prolonged survival. Cuprizone did not inhibit cell proliferation, but probably inhibited tumor cell invasion. Cuprizone treatment was accompanied by a recruitment of CD68-positive cells.

7. FUTURE PERSPECTIVES

This study identifies glioma cell-myelin sheaths interactions as targets for glioma therapy. However, the therapeutic potential of Cuprizone itself may be limited due to its destructive effect on the myelin. Thus, finding novel compounds that block the attachment of glioma cells to the myelin without causing structural injury should be a goal for future work. Since these efforts will require animal experiments, we believe the model presented here can provide a valuable tool for such studies. However, using this animal model to its full potential will also require dedicated MRI imaging sequences that can monitor tumor cell invasion in vivo. Thus anti-invasive studies will also require that new imaging tools are developed that are optimised and dedicated towards a detailed imaging of tumor invasion.

8. REFERENCES

1. Phebus LA, Johnson KW. Dural inflammation model of migraine pain. Curr Protoc Neurosci. 2001 May;Chapter 9:Unit9 1.
2. Pecorino L. Molecular biology of cancer : mechanisms, targets, and therapeutics / Lauren Pecorino. 2nd ed2008.
3. Chen S, Sang N. Histone deacetylase inhibitors: the epigenetic therapeutics that repress hypoxia-inducible factors. J Biomed Biotechnol. 2011;2011:197946.
4. Stein GS, van Wijnen AJ, Imbalzano AN, Montecino M, Zaidi SK, Lian JB, et al. Architectural genetic and epigenetic control of regulatory networks: compartmentalizing machinery for transcription and chromatin remodeling in nuclear microenvironments. Crit Rev Eukaryot Gene Expr. 2010;20(2):149-55.
5. Park YJ, Claus R, Weichenhan D, Plass C. Genome-wide epigenetic modifications in cancer. Prog Drug Res. 2011;67:25-49.
6. Stratton MR. Exploring the genomes of cancer cells: progress and promise. Science. 2011 Mar 25;331(6024):1553-8.
7. Pietras K, Ostman A. Hallmarks of cancer: interactions with the tumor stroma. Exp Cell Res. 2010 May 1;316(8):1324-31.
8. Hanahan D, Weinberg RA. Hallmarks of cancer: the next generation. Cell. [Research Support, N.I.H., Extramural
Review]. 2011 Mar 4;144(5):646-74.
9. Hanahan D, Weinberg RA. The hallmarks of cancer. Cell. [Research Support, U.S. Gov't, Non-P.H.S.
Research Support, U.S. Gov't, P.H.S.
Review]. 2000 Jan 7;100(1):57-70.
10. Gahn B, Schafer C, Neef J, Troff C, Feuring-Buske M, Hiddemann W, et al. Detection of trisomy 12 in CD34+ progenitor cells in a patient with B-cell chronic lymphocytic leukemia by fluorescence in situ hybridization. Ann Oncol. 1997;8 Suppl 2:55-7.
11. Li LJ, Fu R, Shao ZH, Wang HQ, Yue LZ, Ruan EB, et al. [Abnormalities of CD34+ cells differentiation and bone marrow cell cycle in myelodysplastic syndrome]. Zhonghua Nei Ke Za Zhi. 2010 Nov;49(11):963-6.
12. Rego EM, Garcia AB, Carneiro JJ, Falcao RP. Immunophenotype of normal and leukemic bone marrow B-precursors in a Brazilian population. A comparative analysis by quantitative fluorescence cytometry. Braz J Med Biol Res. 2001 Feb;34(2):183-94.
13. Bao S, Wu Q, Sathornsumetee S, Hao Y, Li Z, Hjelmeland AB, et al. Stem cell-like glioma cells promote tumor angiogenesis through vascular endothelial growth factor. Cancer Res. [Research Support, Non-U.S. Gov't]. 2006 Aug 15;66(16):7843-8.
14. Altaner C. Glioblastoma and stem cells. Neoplasma. 2008;55(5):369-74.
15. Bidlingmaier S, Zhu X, Liu B. The utility and limitations of glycosylated human CD133 epitopes in defining cancer stem cells. J Mol Med. 2008 Sep;86(9):1025-32.
16. Dell'Albani P. Stem cell markers in gliomas. Neurochem Res. 2008 Dec;33(12):2407-15.
17. Perez Castillo A, Aguilar-Morante D, Morales-Garcia JA, Dorado J. Cancer stem cells and brain tumors. Clin Transl Oncol. 2008 May;10(5):262-7.
18. Woodward WA, Sulman EP. Cancer stem cells: markers or biomarkers? Cancer Metastasis Rev. 2008 Sep;27(3):459-70.
19. Prestegarden L, Svendsen A, Wang J, Sleire L, Skaftnesmo KO, Bjerkvig R, et al. Glioma cell populations grouped by different cell type markers drive brain tumor growth. Cancer Res. 2010 Jun 1;70(11):4274-9.

20. Singh SK, Hawkins C, Clarke ID, Squire JA, Bayani J, Hide T, et al. Identification of human brain tumour initiating cells. Nature. 2004 Nov 18;432(7015):396-401.
21. Singh SK, Clarke ID, Terasaki M, Bonn VE, Hawkins C, Squire J, et al. Identification of a cancer stem cell in human brain tumors. Cancer Res. 2003 Sep 15;63(18):5821-8.
22. Stupp R, Mason WP, van den Bent MJ, Weller M, Fisher B, Taphoorn MJ, et al. Radiotherapy plus concomitant and adjuvant temozolomide for glioblastoma. N Engl J Med. 2005 Mar 10;352(10):987-96.
23. Kleihues P, Burger PC, Scheithauer BW. The new WHO classification of brain tumours. Brain Pathol. 1993 Jul;3(3):255-68.
24. Adamson C, Kanu OO, Mehta AI, Di C, Lin N, Mattox AK, et al. Glioblastoma multiforme: a review of where we have been and where we are going. Expert Opin Investig Drugs. 2009 Aug;18(8):1061-83.
25. Ohgaki H, Kleihues P. Genetic pathways to primary and secondary glioblastoma. Am J Pathol. 2007 May;170(5):1445-53.
26. Brem SS, Bierman PJ, Brem H, Butowski N, Chamberlain MC, Chiocca EA, et al. Central nervous system cancers. J Natl Compr Canc Netw. 2011 Apr;9(4):352-400.
27. Burger PC, Scheithauer BW, Kleihues P. Histological types of tumours of the central nervous system 1993.
28. Louis DN, Ohgaki H, Wiestler OD, Cavenee WK, Burger PC, Jouvet A, et al. The 2007 WHO classification of tumours of the central nervous system. Acta Neuropathol. 2007 Aug;114(2):97-109.
29. Network CGAR. Comprehensive genomic characterization defines human glioblastoma genes and core pathways. Nature. 2008 Oct 23;455(7216):1061-8.
30. Verhaak RG, Hoadley KA, Purdom E, Wang V, Qi Y, Wilkerson MD, et al. Integrated genomic analysis identifies clinically relevant subtypes of glioblastoma characterized by abnormalities in PDGFRA, IDH1, EGFR, and NF1. Cancer Cell. 2010 Jan 19;17(1):98-110.
31. Mischel PS, Nelson SF, Cloughesy TF. Molecular analysis of glioblastoma: pathway profiling and its implications for patient therapy. Cancer Biol Ther. 2003 May-Jun;2(3):242-7.
32. Pilkington CJ. The role of the extracellular matrix in neoplastic glial invasion of the nervous system. Braz J Med Biol Res. 1996 Sep;29(9):1159-72.
33. Giese A, Westphal M. Glioma invasion in the central nervous system. Neurosurgery. 1996 Aug;39(2):235-50; discussion 50-2.
34. Montana V, Sontheimer H. Bradykinin promotes the chemotactic invasion of primary brain tumors. J Neurosci. 2011 Mar 30;31(13):4858-67.
35. De Clerck YA, Shimada H, Gonzalez-Gomez I, Raffel C. Tumoral invasion in the central nervous system. J Neurooncol. 1994;18(2):111-21.
36. Giese A, Kluwe L, Laube B, Meissner H, Berens ME, Westphal M. Migration of human glioma cells on myelin. Neurosurgery. 1996 Apr;38(4):755-64.
37. Tysnes BB, Mahesparan R. Biological mechanisms of glioma invasion and potential therapeutic targets. J Neurooncol. 2001 Jun;53(2):129-47.
38. Kitai R, Horita R, Sato K, Yoshida K, Arishima H, Higashino Y, et al. Nestin expression in astrocytic tumors delineates tumor infiltration. Brain Tumor Pathol. 2010 Apr;27(1):17-21.
39. Wesseling P, Ruiter DJ, Burger PC. Angiogenesis in brain tumors; pathobiological and clinical aspects. J Neurooncol. 1997 May;32(3):253-65.
40. Lakomy R, Burkon P, Burkonova D, Jancalek R. [New therapeutic options in therapy of glioblastoma multiforme]. Klin Onkol. 2010;23(6):381-7.
41. Kanu OO, Mehta A, Di C, Lin N, Bortoff K, Bigner DD, et al. Glioblastoma multiforme: a review of therapeutic targets. Expert Opin Ther Targets. 2009 Jun;13(6):701-18.

42. Fan QW, Weiss WA. Targeting the RTK-PI3K-mTOR axis in malignant glioma: overcoming resistance. Curr Top Microbiol Immunol. 2010;347:279-96.
43. Bo L, Vedeler CA, Nyland HI, Trapp BD, Mork SJ. Subpial demyelination in the cerebral cortex of multiple sclerosis patients. J Neuropathol Exp Neurol. 2003 Jul;62(7):723-32.
44. Donaghy M. Brain's Diseases of the Nervous system. 12th ed2009.
45. Hauser Stephen L GDS. Principles of Internal Medicine. Available from: http://www.accessmedicine.com/content.aspx?aID=2906445. .
46. Norsk Helse D. Multiple sclerosis. 2011; Available from: www.helse.biblioteket.no.
47. Marrie RA. Environmental risk factors in multiple sclerosis aetiology. Lancet Neurol. 2004 Dec;3(12):709-18.
48. Torkildsen O, Brunborg LA, Myhr KM, Bo L. The cuprizone model for demyelination. Acta Neurol Scand Suppl. [Review]. 2008;188:72-6.
49. Trapp BD, Bo L, Mork S, Chang A. Pathogenesis of tissue injury in MS lesions. J Neuroimmunol. 1999 Jul 1;98(1):49-56.
50. Hafler DA, Slavik JM, Anderson DE, O'Connor KC, De Jager P, Baecher-Allan C. Multiple sclerosis. Immunol Rev. 2005 Apr;204:208-31.
51. Kirk J, Plumb J, Mirakhur M, McQuaid S. Tight junctional abnormality in multiple sclerosis white matter affects all calibres of vessel and is associated with blood-brain barrier leakage and active demyelination. J Pathol. 2003 Oct;201(2):319-27.
52. Rolak LA. Multiple sclerosis: it's not the disease you thought it was. Clin Med Res. 2003 Jan;1(1):57-60.
53. Trapp BD, Peterson J, Ransohoff RM, Rudick R, Mork S, Bo L. Axonal transection in the lesions of multiple sclerosis. N Engl J Med. 1998 Jan 29;338(5):278-85.
54. Compston A, Coles A. Multiple sclerosis. Lancet. 2002 Apr 6;359(9313):1221-31.
55. Compston A, Coles A. Multiple sclerosis. Lancet. 2008 Oct 25;372(9648):1502-17.
56. Forbund NM. Multiple sclerosis. 2011; Available from: www.MS-forbund.no.
57. Matsushima GK, Morell P. The neurotoxicant, cuprizone, as a model to study demyelination and remyelination in the central nervous system. Brain Pathol. 2001 Jan;11(1):107-16.
58. Schwentker FF, Rivers TM, Finkelstein MH. OBSERVATIONS ON THE IMMUNOLOGICAL RELATION OF POLIOMYELITIS TO LOUPING ILL. J Exp Med. 1933 May 31;57(6):955-65.
59. Blakemore WF. Remyelination of the superior cerebellar peduncle in old mice following demyelination induced by cuprizone. J Neurol Sci. [Comparative Study]. 1974 May;22(1):121-6.
60. Rodriguez M. Effectors of demyelination and remyelination in the CNS: implications for multiple sclerosis. Brain Pathol. [Research Support, N.I.H., Extramural
Research Support, Non-U.S. Gov't
Review]. 2007 Apr;17(2):219-29.
61. Koutsoudaki PN, Skripuletz T, Gudi V, Moharregh-Khiabani D, Hildebrandt H, Trebst C, et al. Demyelination of the hippocampus is prominent in the cuprizone model. Neurosci Lett. 2009 Feb 13;451(1):83-8.
62. Skripuletz T, Bussmann JH, Gudi V, Koutsoudaki PN, Pul R, Moharregh-Khiabani D, et al. Cerebellar cortical demyelination in the murine cuprizone model. Brain Pathol. 2010 Mar;20(2):301-12.
63. Xu H, Yang HJ, Zhang Y, Clough R, Browning R, Li XM. Behavioral and neurobiological changes in C57BL/6 mice exposed to cuprizone. Behav Neurosci. 2009 Apr;123(2):418-29.

64. Messori L, Casini A, Gabbiani C, Sorace L, Muniz-Miranda M, Zatta P. Unravelling the chemical nature of copper cuprizone. Dalton Trans. 2007 Jun 7(21):2112-4.
65. Kipp M, Clarner T, Dang J, Copray S, Beyer C. The cuprizone animal model: new insights into an old story. Acta Neuropathol. [Research Support, Non-U.S. Gov't]. 2009 Dec;118(6):723-36.
66. Taylor LC, Gilmore W, Matsushima GK. SJL mice exposed to cuprizone intoxication reveal strain and gender pattern differences in demyelination. Brain Pathol. 2009 Jul;19(3):467-79.
67. McMahon EJ, Cook DN, Suzuki K, Matsushima GK. Absence of macrophage-inflammatory protein-1alpha delays central nervous system demyelination in the presence of an intact blood-brain barrier. J Immunol. 2001 Sep 1;167(5):2964-71.
68. McMahon EJ, Suzuki K, Matsushima GK. Peripheral macrophage recruitment in cuprizone-induced CNS demyelination despite an intact blood-brain barrier. J Neuroimmunol. 2002 Sep;130(1-2):32-45.
69. Morell P, Barrett CV, Mason JL, Toews AD, Hostettler JD, Knapp GW, et al. Gene expression in brain during cuprizone-induced demyelination and remyelination. Mol Cell Neurosci. 1998 Nov;12(4-5):220-7.
70. Norkute A, Hieble A, Braun A, Johann S, Clarner T, Baumgartner W, et al. Cuprizone treatment induces demyelination and astrocytosis in the mouse hippocampus. J Neurosci Res. 2009 May 1;87(6):1343-55.
71. Skripuletz T, Miller E, Moharregh-Khiabani D, Blank A, Pul R, Gudi V, et al. Beneficial effects of minocycline on cuprizone induced cortical demyelination. Neurochem Res. 2010 Sep;35(9):1422-33.
72. Sun SW, Liang HF, Trinkaus K, Cross AH, Armstrong RC, Song SK. Noninvasive detection of cuprizone induced axonal damage and demyelination in the mouse corpus callosum. Magn Reson Med. 2006 Feb;55(2):302-8.
73. Taylor LC, Gilmore W, Ting JP, Matsushima GK. Cuprizone induces similar demyelination in male and female C57BL/6 mice and results in disruption of the estrous cycle. J Neurosci Res. 2010 Feb 1;88(2):391-402.
74. Torkildsen O, Brunborg LA, Thorsen F, Mork SJ, Stangel M, Myhr KM, et al. Effects of dietary intervention on MRI activity, de- and remyelination in the cuprizone model for demyelination. Exp Neurol. 2009 Jan;215(1):160-6.
75. Suzuki K, Kikkawa Y. Status spongiosus of CNS and hepatic changes induced by cuprizone (biscyclohexanone oxalyldihydrazone). Am J Pathol. 1969 Feb;54(2):307-25.
76. Lindner M, Fokuhl J, Linsmeier F, Trebst C, Stangel M. Chronic toxic demyelination in the central nervous system leads to axonal damage despite remyelination. Neurosci Lett. 2009 Apr 3;453(2):120-5.
77. Miron VE, Kuhlmann T, Antel JP. Cells of the oligodendroglial lineage, myelination, and remyelination. Biochim Biophys Acta. 2011 Feb;1812(2):184-93.
78. Gudi V, Moharregh-Khiabani D, Skripuletz T, Koutsoudaki PN, Kotsiari A, Skuljec J, et al. Regional differences between grey and white matter in cuprizone induced demyelination. Brain Res. 2009 Aug 4;1283:127-38.
79. Miller et al. Multiple sclerosis. 2006.
80. Jin K, Teng L, Shen Y, He K, Xu Z, Li G. Patient-derived human tumour tissue xenografts in immunodeficient mice: a systematic review. Clin Transl Oncol. [Research Support, Non-U.S. Gov't
Review]. 2010 Jul;12(7):473-80.
81. Troiani T, Schettino C, Martinelli E, Morgillo F, Tortora G, Ciardiello F. The use of xenograft models for the selection of cancer treatments with the EGFR as an example. Crit Rev Oncol Hematol. [Review]. 2008 Mar;65(3):200-11.

82. Morton CL, Houghton PJ. Establishment of human tumor xenografts in immunodeficient mice. Nat Protoc. 2007;2(2):247-50.
83. Ishikawa F. ["Creation of mouse models for human diseases"]. Nihon Rinsho Meneki Gakkai Kaishi. [Review]. 2010;33(6):304-11.
84. FELASA Working Group on Animal Health L. FELASA recommendations for the health
monitoring of mouse, rat, hamster, gerbil,
guineapig and rabbit experimental units. 1996 [cited 2011 15/06]; Available from: http://la.rsmjournals.com/cgi/reprint/30/3/193.pdf.
85. Bjerkvig R, Tonnesen A, Laerum OD, Backlund EO. Multicellular tumor spheroids from human gliomas maintained in organ culture. J Neurosurg. 1990 Mar;72(3):463-75.
86. Lindner M, Heine S, Haastert K, Garde N, Fokuhl J, Linsmeier F, et al. Sequential myelin protein expression during remyelination reveals fast and efficient repair after central nervous system demyelination. Neuropathol Appl Neurobiol. 2008 Feb;34(1):105-14.
87. Dhaked RK, Singh MK, Singh P, Gupta P. Botulinum toxin: bioweapon & magic drug. Indian J Med Res. 2010 Nov;132(5):489-503.
88. Molenaers G, Van Campenhout A, Fagard K, De Cat J, Desloovere K. The use of botulinum toxin A in children with cerebral palsy, with a focus on the lower limb. J Child Orthop. 2010 Jun;4(3):183-95.
89. Breccia M, Cicconi L, Minotti C, Latagliata R, Gianni L, Lo-Coco F. Efficacy of prolonged therapy with combined arsenic trioxide and ATRA for relapse of acute promyelocytic leukemia. Haematologica. 2011 Jun 9.
90. Mason JL, Toews A, Hostettler JD, Morell P, Suzuki K, Goldman JE, et al. Oligodendrocytes and progenitors become progressively depleted within chronically demyelinated lesions. Am J Pathol. 2004 May;164(5):1673-82.
91. HJ S. The forms of growth in gliomas and their practical significance. Brain 63:1–35, 1940. 1940.